THE ASTROPHYSICAL JOURNAL, **216**:291–307, 1977 August 15

A SURVEY OF INTERSTELLAR MOLECULAR HYDROGEN. I.

B. D. SAVAGE,*† R. C. BOHLIN,*‡ J. F. DRAKE,§ AND W. BUDICH||
Received 1977 January 17

ABSTRACT

The *Copernicus* ultraviolet telescope was used to survey the column densities of interstellar H_2 in the $J = 0$ and 1 rotational levels of the $v'' = 0$ vibrational state toward 109 stars, including 26 measurements collected from previous publications. In most cases, the H_2 lines exhibit strong damping wings; and column densities are derived by fitting damping profiles to the observed spectra. For stars with strong H_2 lines, most of the interstellar H_2 is in the two lowest rotational levels; and $N(0) + N(1)$ is a good measure of $N(H_2)$, the total H_2 column density. When $f = 2N(H_2)/[2N(H_2) + N(\text{H I})]$ is correlated with $E(B - V)$ and with $N(\text{H I} + H_2)$, the total hydrogen column density, it is found that f undergoes a transition from low values (<0.01) to high values (>0.01) when $E(B - V) \approx 0.08$ and $N(\text{H I} + H_2) \approx 5 \times 10^{20}$ atoms cm^{-2}. For $E(B - V) < 0.15$, 88% of the stars observed have $f < 0.1$, while for $E(B - V) \geq 0.15$, 74% have $f \geq 0.1$. The correlations of f with $E(B - V)$ or $N(\text{H I} + H_2)$ show a peak-to-peak spread of about a factor of 10 in the values of f. For stars with $E(B - V) \geq 0.1$, the smaller than normal values of f are often associated with objects which have a larger than normal gas-to-color excess ratio. The observed trends are consistent with recent theoretical calculations of J. Black involving a balance between the efficient formation of H_2 on interstellar grains and the destruction of H_2 through a two-step photodissociation process in clouds with total densities ranging from about 10 to 500 atoms cm^{-3}. A group of five stars with middle B spectral types and with small $E(B - V)$ exhibit abnormally large values of $N(H_2)$. Three of these stars also have unusually strong CH^+ lines, possibly suggesting a common circumstellar origin for the two molecules. The survey measurements provide the following overall averages: $\langle n(H_2)\rangle = \sum N(H_2)/\sum r = 0.036$ cm^{-3}, $\langle n(\text{H I})\rangle = \sum N(\text{H I})/\sum r = 0.35$ cm^{-3}, and $\langle f\rangle = 2\langle n(H_2)\rangle/[2\langle n(H_2)\rangle + \langle n(\text{H I})\rangle] = 0.17$. However, these results are strongly influenced by sampling biases. After correcting for these biases, the following averages are obtained for matter in the galactic plane within 500 pc of the Sun: $\langle n(H_2)\rangle = 0.143$ cm^{-3}, $\langle n(\text{H I})\rangle = 0.86$ cm^{-3}, and $\langle f\rangle = 0.25$. For stars with $N(H_2)$ larger than 10^{18} atoms cm^{-2}, the $N(1)/N(0)$ population ratio provides a direct measure of cloud kinetic temperatures. The values of T_{01} range from 45 to 128 K, with an average over 61 stars of 77 ± 17 (rms) K.

Subject headings: interstellar: abundances — interstellar: matter — interstellar: molecules

I. INTRODUCTION

The hydrogen molecule plays a central role in a variety of processes that significantly influence the chemical and physical state of the interstellar medium. Because of the great importance of this molecule to an eventual understanding of diffuse and dense interstellar clouds, the *Copernicus* satellite was used to survey the column densities of atomic and molecular hydrogen toward a large sample of early-type stars. The results for H I are presented by Bohlin, Savage, and Drake (1977, hereafter Paper II). In this paper (Paper I) we derive new column densities or upper limits for interstellar H_2 in the $J = 0$ and 1 rotational levels, $N(0)$ and $N(1)$, of the ground vibrational state toward 70 stars. In general, the stars studied are more distant or more reddened than those studied previously (Carruthers 1970; Smith 1973*a*; Spitzer *et al.* 1973; Spitzer, Cochran, and Hirschfeld 1974; Morton and Dinerstein 1976; York 1976). In addition, revisions to preliminary values of $N(0)$ and $N(1)$ are presented for 13 stars. When combined with the earlier *Copernicus* results, H_2 column densities or upper limits now exist for 109 stars (Table 1). Although the new measurements are restricted to the levels $J = 0$ and 1, $N(0) + N(1)$ is a reliable measure of the total interstellar H_2 column density, since most of the new stars have at least 99% of the interstellar H_2 in the two lowest rotational levels.

In § II we discuss the observations, data reduction, and probable errors. The results are described in § III.

* Guest Investigator with the Princeton University telescope on the *Copernicus* satellite, which is sponsored and operated by the National Aeronautics and Space Administration.

† Washburn Observatory, University of Wisconsin, Madison.

‡ Goddard Space Flight Center.

§ Lockheed Palo Alto Research Laboratory.

|| Computer Sciences Corporation.

II. OBSERVATIONS AND DATA REDUCTION

a) The Observing Program

In order to gain more information about the space distribution of interstellar H_2, stars were surveyed at greater distances or with larger $(B - V)$ excesses than

TABLE 1

THE RESULTS

1	2	3	4	5	6	7	8	9	10	11	12	13	14	15	16	17
HD	NAME	ℓ^{II}	b^{II}	S. T.	E(B-V) mag.	r [pc]	log N(0) [cm^{-2}]	log N(1) [cm^{-2}]	log error	log N(H_2) [cm^{-2}]	log N(HI) [cm^{-2}]	log N(HI + H_2) [cm^{-2}]	log f	T_{01} [K]	n(HI + H_2) [cm^{-3}]	Comments
886	γ Peg	109	-47	B2 IV	.01	145	<12.8	-	-	<14.2	20.04	20.04	<-5.54	-	.25	3
2905	κ Cas	121	0	B1 Ia	.35	1009	19.83	20.08	.18	20.27	21.20	21.30	-.72	104	.64	1
5394	γ Cas	124	-2	B0.5 IVpe	.08	194	<17.1	<17.3	-	<17.51	20.16	20.16	<-2.36	-	.24	2D
10144	α Eri	291	-59	B3 Vp	.04	22	<12.5	-	-	<13.9	-	-	-	-	-	3
10516	φ Per	131	-11	B2 Vpe	.20	137	18.90	18.60	.18	19.08	20.54	20.57	-1.19	59	.88	2
14228	φ Eri	275	-61	B8 V	.00	62	<16.4	<16.7	-	<17.0	-	-	-	-	-	2N
14633		141	-18	ON8 V	.10	2042	<18.70	<18.90	-	<19.11	20.56	20.56	<-1.17	-	.058	1D
21278		148	-6	B4 V	.10	143	19.23	19.11	.23	19.48	-	-	-	73	-	2R
21856		156	-17	B1 V	.19	581	19.70	19.78	.15	20.04	21.04	21.12	-.77	84	.74	1
22928	δ Per	150	-6	B5 III	.01	82	18.93	19.08	.20	19.30	-	>19.60	-	92	>.15	2R
22951	40 Per	159	-17	B1 IV	.24	406	20.26	20.04	.18	20.46	21.04	21.23	-.46	63	1.3	1
23180	ο Per	160	-18	B1 III	.30	239	20.51	19.93	.15	20.61	20.90	21.21	-.30	48	2.2	2
23408	20 Tau	166	-24	B8 III	.00	78	19.38	19.51	.26	19.75	-	>20.05	-	89	>.46	*2
23480	23 Tau	167	-24	B6 IV	.08	81	19.89	19.72	.18	20.12	-	>20.42	-	67	>1.1	*2
23630	η Tau	167	-23	B7 III	.00	59	19.20	19.28	.18	19.54	-	>19.84	-	84	>.38	*2
24398	ζ Per	162	-17	B1 Ib	.33	394	20.51	20.18	.18	20.67	20.81	21.20	-.23	57	1.3	2R
24760	ε Per	157	-10	B0.5 III	.09	308	19.20	19.24	.26	19.53	20.40	20.50	-.67	81	.34	2R
24912	ξ Per	160	-13	O7.5 IIInf	.33	538	20.34	20.09	.15	20.53	21.11	21.30	-.46	61	1.2	2R
28497		209	-37	B1.5 Ve	.02	466	13.90	14.50	-	14.82	20.20	20.20	-5.08	212	.11	5
30614	α Cam	144	14	O9.5 Ia	.32	1164	20.02	20.05	.15	20.34	20.90	21.09	-.45	80	.35	2R
34989		195	-16	B1 V	.13	603	<18.11	<18.18	-	<18.45	21.11	21.11	<-2.36	-	.69	1D
35149	23 Ori	199	-18	B1 Vn	.11	429	<18.15	<18.30	-	<18.53	20.74	20.74	<-1.91	-	.42	1D
36486	δ Ori	204	-18	O9.5 II	.07	384	13.54	14.45	-	14.68	20.23	20.23	-5.25	1625	.14	4
36822	ϕ^1 Ori	195	-13	B0.5 IV-V	.11	413	19.11	18.90	.15	19.32	20.81	20.84	-1.21	63	.54	1
36861	λ Ori	195	-12	O8 IIIf	.12	532	19.04	18.34	.20	19.11	20.78	20.80	-1.38	45	.38	2R
37022	θ^1 Ori C	209	-19	O7:	.31	550	<17.3	<17.2	-	<17.55	21.04	21.04	<-3.22	-	.65	*2N
37043	ι Ori	210	-20	O9 III	.07	429	13.60	14.40	-	14.69	20.15	20.15	-5.16	463	.11	4
37128	ε Ori	205	-17	B0 Ia	.08	409	16.08	16.36	-	16.57	20.45	20.45	-3.59	108	.22	4
37202	ζ Tau	186	-6	B2 IVp	.05	145	<16.7	<17.6	-	<17.67	20.04	20.04	<-2.1	-	.25	2N
37742	ζ Ori	206	-17	O9.7 Ib	.08	352	15.22	15.45	-	15.73	20.41	20.41	-4.38	101	.24	4
38666	μ Col	237	-27	O9.5 V	.01	701	15.05	15.24	-	15.51	19.85	19.85	-4.04	96	.032	4
38771	κ Ori	215	-19	B0.5 Ia	.07	520	15.01	15.49	-	15.68	20.52	20.52	-4.54	156	.21	4
40111	139 Tau	184	1	B1 Ib	.15	1247	19.24	19.56	.20	19.74	20.90	20.96	-.92	117	.24	2R
44743	β CMa	226	-14	B1 II-III	.00	206	<17.0	<17.1	-	<17.3	<18.70	<18.73	-	-	<.0084	2N
47129		206	0	O8 p	.36	752	20.30	20.18	.18	20.54	21.08	21.28	-.43	68	.82	1
47839	15 Mon	203	2	O7 Vf	.07	705	14.52	15.41	-	15.55	20.40	20.40	-4.55	1153	.12	4
48099		206	1	O7 V	.27	1169	19.88	20.08	.15	20.29	21.15	21.25	-.66	98	.50	1
50896		235	-10	WN5 + B	.14	1393	19.00	19.00	.11	19.30	20.54	20.59	-1.00	77	.091	1
52089	ε CMa	240	-11	B2 II	.01	188	<17.4	<17.3	-	<17.66	<18.7	<18.77	-	-	<.010	2N
53975		226	-2	O7.5 V	.22	1334	18.70	19.08	.18	19.23	21.15	21.16	-1.62	128	.35	1
54662		224	-1	O6.5 V	.35	1236	19.60	19.78	.18	20.00	21.38	21.41	-1.11	95	.68	1
55879		225	0	B0 III	.10	1462	<18.48	<18.70	-	<18.90	20.90	20.90	<-1.70	-	.18	1D
57060	29 CMa	238	-5	O7Ia: fp	.18	1871	15.36	15.42	-	15.78	20.70	20.70	-4.62	82	.087	4
57061	30 CMa	238	-6	O9 II	.15	933	14.40	15.21	-	15.47	20.70	20.70	-4.92	513	.17	4
57682		224	3	O9 IV	.12	1614	<18.48	<18.78	-	<18.95	20.87	20.87	<-1.62	-	.15	1D
66811	ζ Pup	256	-5	O4 Inf	.05	668	13.14	13.90	-	14.45	19.99	19.99	-5.23	378	.047	6
68273	γ^2 Vel	263	-8	O9I + WN8	.05	377	12.98	13.80	-	14.23	19.78	19.78	-5.25	544	.052	4
74375		276	-11	B1.5 III	.10	348	<18.00	<18.08	-	<18.34	20.82	20.82	<-2.18	-	.62	1D
87901	α Leo	226	49	B7 V	.00	24	<13.9	<14.6	-	<14.98	-	-	-	-	-	2N
91316	ρ Leo	235	53	B1 Iab	.08	959	14.63	15.39	-	15.61	20.26	20.26	-4.35	377	.061	4
92740		287	-1	WN7	.33	2780	19.63	19.70	.15	19.97	21.20	21.25	-.98	83	.21	2
93030	θ Car	290	-5	B0.5 Vp	.06	207	<16.8	<17.6	-	<17.65	20.28	20.28	<-2.32	-	.30	2D
93521		183	62	O9 Vp	.03	1778	<17.95	<18.42	-	<18.54	20.11	20.11	<-1.27	-	.023	*1D
99171		286	17	B2 IV-V	.05	470	14.37	14.82	.15	15.25	20.65	20.65	-5.10	146	.31	*1
112244		304	6	O8.5 Iaf	.34	1854	19.80	19.88	.11	20.14	21.08	21.17	-.73	84	.26	1
113904B	θ Mus	305	-2	O9 II	.29	1276	19.41	19.62	.11	19.83	21.08	21.13	-1.00	99	.34	1
116658	α Vir	316	51	B1 IV	.03	86	<11.9	12.7	-	12.95	<19.0	<19.0	-	-	<.038	5
120315	η UMa	101	65	B3 V	.02	42	<12.5	<12.7	-	13.38	-	-	-	-	-	5
121263	ζ Cen	314	14	B2.5 IV	.00	85	<12.5	12.8	-	12.8	<20.02	<20.02	-	-	<.40	5
122451	β Cen	312	1	B1 III	.00	84	<11.9	12.8	-	12.8	19.52	19.52	-5.42	-	.13	5
125823	a Cen	322	20	B7 IIIp	.00	121	<17.2	<17.9	-	<17.99	-	-	-	-	-	2N
135591		320	-3	O7.5 IIIf	.22	1178	19.53	19.40	.11	19.77	21.08	21.12	-1.05	68	.36	1
135742	β Lib	352	39	B8 V	.00	40	<13.4	<13.7	-	<14.35	-	-	-	-	-	5
141637	1 Sco	346	22	B1.5 Vn	.20	232	18.95	18.90	.18	19.23	21.19	21.20	-1.67	73	2.2	1
143018	π Sco	347	20	B1 V + B2	.08	171	19.00	19.04	.20	19.32	20.72	20.75	-1.13	81	1.1	2
143275	δ Sco	350	23	B0.5 IV	.16	155	19.26	18.90	.20	19.41	21.15	21.16	-1.45	56	3.0	2
144217A	β^1 Sco	353	24	B0.5 V	.20	161	19.46	19.58	.06	19.83	21.09	21.14	-1.01	88	2.8	1
144470	ω^1 Sco	353	23	B1 V	.22	227	19.78	19.72	.11	20.05	21.18	21.24	-.89	73	2.5	1
145502	ν Sco	355	23	B2 IVp	.27	174	19.52	19.65	.15	19.89	21.15	21.19	-1.00	90	2.9	1
147165	σ Sco	351	17	B1 III	.38	142	19.57	19.38	.15	19.79	21.34	21.37	-1.28	64	5.3	*1, 2
147933A	ρ Oph	354	18	B2 IV	.47	174	20.48	19.85	.15	20.57	21.81	21.86	-1.00	46	13.	1
148184	χ Oph	358	21	B1.5 Ve	.53	134	20.54	19.90	.18	20.63	21.15	21.35	-.42	46	5.5	1
148605	22 Sco	353	16	B2 V	.10	217	18.54	18.30	.18	18.74	20.95	20.96	-1.92	61	1.4	1
149038	μ Nor	339	3	O9.7 Iab	.38	1122	20.30	19.89	.15	20.44	21.00	21.19	-.45	54	.45	2
149438	τ Sco	352	13	B0 V	.06	236	<13.22	14.07	-	14.50	20.49	20.49	-5.70	-	.42	4

TABLE 1 (continued)

1 HD	2 NAME	3 ℓ^{II}	4 b^{II}	5 S. T.	6 E(B-V) mag.	7 r [pc]	8 log N(0) [cm^{-2}]	9 log N(1) [cm^{-2}]	10 log error	11 log $N(H_2)$ [cm^{-2}]	12 log N(HI) [cm^{-2}]	13 log $N(HI + H_2)$ [cm^{-2}]	14 log f	15 T_{01} [K]	16 $n(HI + H_2)$ [cm^{-3}]	17 Comments
149757	ζ Oph	6	24	09.5 Vnn	.32	138	20.51	20.10	.08	20.65	20.72	21.15	-.20	54	3.3	*1,2R
149881		31	36	B0.5 III	(.12)	1614	<18.70	<18.70	-	<19.00	20.65	20.65	<-1.35	-	.090	*1D
150898		330	-8	B0.5 Ia	.18	2323	19.53	19.48	.18	19.81	20.95	21.01	.90	73	.14	1
151804		344	2	08 Iaf	.40	1795	19.95	19.95	.11	20.26	21.08	21.19	-.63	77	.28	1
152408		344	1	08: Iafpe	.48	1888	20.04	20.11	.18	20.38	21.26	21.36	-.68	84	.39	2
155806		353	3	07.5 Vne	.33	735	19.64	19.60	.15	19.92	21.08	21.14	-.91	74	.60	1
157246	γ Ara	335	-11	B1 Ib	.08	689	18.93	18.94	.23	19.24	20.68	20.71	-1.18	79	.24	2R
158408	υ Sco	351	-2	B2 IV	.02	134	<12.7	-	-	<14.1	<19.26	<19.26	-	-	<.043	3
158926	λ Sco	352	-2	B1.5 IV	.03	102	<12.0	12.7	-	12.7	19.38	19.38	-6.38	-	.076	5
164353	67 Oph	30	13	B5 Ib	.12	762	19.98	19.94	.28	20.26	21.00	21.14	-.57	75	.58	2R
164402		7	0	B0 Ib	.28	1738	19.04	19.30	.18	19.49	21.11	21.13	-1.34	106	.25	1
165024	θ Ara	343	-14	B2 Ib	.10	745	<18.78	<18.48	.11	<18.95	20.85	20.85	<-1.60	-	.31	1D
167263	16 Sgr	11	-2	09.5II-IIIn	.31	1349	19.85	19.91	.18	20.18	21.08	21.18	-.69	83	.36	1
167264	15 Sgr	10	-2	B0 Ia	.34	1556	19.98	19.98	.10	20.28	21.15	21.25	-.67	77	.37	1
175191	σ Sgr	10	-12	B3 IV	.00	57	<12.6	-	-	<14.0	<19.48	<19.48	-	-	<.17	3
184915	κ Aql	32	-13	B0.5 IIIn	.26	630	20.06	19.95	.15	20.31	20.90	21.08	-.47	69	.62	1
186994		79	10	B0.2 IV	(.00)	2355	<19.34	<19.34	-	<19.64	20.90	20.90	<-.96	-	.11	1D
188209		81	10	09.5 Iab	.21	2014	19.72	19.70	.11	20.01	20.90	21.00	-.70	76	.16	1
188439		82	10	B0.5 IIIn	.14	1358	19.78	19.48	.11	19.95	20.78	20.89	-.64	59	.19	1
193322AB		78	3	09 V: n	.40	608	19.78	19.78	.18	20.08	21.08	21.16	-.77	77	.77	1
193924	α Pav	341	-35	B2.5 V	.02	57	<12.9	-	-	<14.3	<19.3	<19.3	-	-	<.11	3
199579		86	0	06 Vf	.36	1086	20.08	20.04	.18	20.36	21.08	21.22	-.55	74	.50	1
200120	59 Cyg	88	1	B1.5 Venn	.18	257	18.95	19.06	.18	19.32	20.26	20.34	-.72	87	.28	2R
203064	68 Cyg	88	-4	07.5 III:nf	.28	893	20.03	19.95	.15	20.29	21.00	21.14	-.55	71	.50	1
204172	69 Cyg	83	-10	B0 Ib	.17	2118	19.30	19.30	.18	19.60	21.00	21.03	-1.13	77	.17	1
209952	α Gru	350	-52	B7 IV	.00	29	<12.8	<13.0	-	<13.68	-	-	-	-	-	5
209975	19 Cep	105	5	09.5 Ib	.38	1086	19.78	19.78	.18	20.08	21.11	21.19	-.80	77	.46	1
210191	35 Aqr	37	-52	B2.5 IV	.07	336	<18.3	<18.3	-	<18.6	<20.66	<20.66	-	-	<.44	*1N
214080		45	-57	B1 Ib	.08	3404	<18.78	<18.60	-	<19.00	20.64	20.64	<-1.34	-	.042	1D
214680	10 Lac	97	-17	09 V	.11	589	18.88	18.95	.11	19.22	20.70	20.73	-1.21	84	.29	*1,2R
217675	o And	102	-16	B6 p	.05	68	19.34	19.40	.18	19.67	-	>19.97	-	82	>.45	2
218376	1 Cas	110	-1	B0.5 III	.22	621	19.81	19.88	.18	20.15	20.95	21.07	-.62	82	.62	1
219188		83	-50	B0.5II-IIIn	(.09)	2355	18.90	19.15	.18	19.34	20.85	20.87	-1.23	103	.10	1
224572	σ Cas	116	-6	B1 V	.17	377	19.90	19.95	.18	20.23	20.88	21.04	-.51	82	.94	1

COMMENT CODE — SOURCES OF THE H_2, N(0) AND N(1) COLUMN DENSITIES

1. This investigation, U1 data.
2. This investigation, U2 data.
3. Upper limit for N(0) from Spitzer et al. (1973). Upper limit for $N(H_2)$ assumes $N(H_2)$ = 23 N(0). This conservative limit is equivalent to a rotational excitation temperature of 1000 K.
4. From Spitzer et al. (1974). Column densities for stars with multiple components have been summed.
5. From York (1976).
6. From Morton and Dinerstein (1976).

D. Denotes data for which only an upper limit is quoted because the damping profile assumption is likely invalid. Lower limits to N(0) and N(1) are approximately 500 times smaller (see §IIb).

R. Denotes revisions of column densities given by Spitzer et al. (1973).

N. Denotes cases where H_2 lines are not detected. Conservative upper limits to N(0) and N(1) are quoted. When log [N(0) + N(1)] < 17, the upper limit to $N(H_2)$ assumes $N(H_2)$ = 2[N(0) + N(1)].

HD — * COMMENTS ABOUT INDIVIDUAL STARS ARE GIVEN BELOW

23408, 23480, 23630: Adams (1949) noted that many of the stars in the Pleiades have abnormally strong CH^+ lines. Hobbs (1972) has recently reported log $N(CH^+)$ = 12.79 and 12.43 for HD 23408 and HD 23480 respectively. The value for HD 23408 is the largest CH^+ column density measured by Hobbs (1973) in a survey of 28 stars.

37022: N(HI) is from Savage and Jenkins (1972). This OAO-2 measurement refers to $\theta^1 + \theta^2$ Ori.

93521: The N(0) and N(1) upper limits derived for this distant, high latitude star are obtained from the (1,0) R(0) and R(1) lines positioned at $V_{Heliocentric} = -2.2 \pm 10$ km s^{-1}. There is no evidence for H_2 absorption lines exceeding 20 mÅ equivalent width over the velocity range -20 to -100 km s^{-1}.

99171: The (1,0) R(0), R(1), and P(1) lines are weak in this star. N(0) and N(1) are derived with the assumption that these lines are on the linear part of the curve of growth. The values of $N(H_2)$ and f assume $N(H_2) \approx$ 2[N(0) + N(1)].

147165: N(0) and N(1) values quoted are from U1 spectra. The U2 spectra yield: log N(0) = 19.58 and log N(1) = 19.36.

149757: N(0) and N(1) values quoted are from U1 spectra. The U2 spectra yield: log N(0) = 20.51 and log N(1) = 20.06.

149881: E(B-V) estimated from photometric data of Stebbins et al. (1940).

165024: The N(1) upper limit is derived from the P(1) line. The (1,0) R(1) line was not scanned.

186994: E(B-V) estimated from photometric data of Stebbins et al. (1940).

210191: H_2 was not detected. The upper limits are large due to severe stellar blending.

214680: N(0) and N(1) values quoted are from U1 spectra. The U2 spectra yield: log N(0) = 18.92 and log N(1) = 18.95.

219188: E(B-V) estimated from photometric data of Stebbins et al. (1940).

in previous *Copernicus* programs (see the review by Spitzer and Jenkins 1975). Since the H_2 measurements can be interpreted better in combination with information on neutral hydrogen, the H_2 observations generally were restricted to stars known to have narrow stellar Lα lines (stars B2 or hotter). However, a number of scans of cooler B stars exhibiting unusual optical interstellar molecular lines were also available, for example 20, 23, and η Tau. These stars were known from the work of Adams (1949) to have unusually strong CH^+ lines. In order to permit studies of variable heavy-element depletion in the interstellar gas, objects with peculiar infrared or far-ultraviolet extinction characteristics were included. Finally, stars from a variety of galactic regions and a few distant high-latitude stars were selected. However, since these ultraviolet interstellar studies are restricted to the use of early-type stars, the distribution of objects is very strongly influenced by the fact that such stars are generally found only in young OB associations located near the galactic plane. Because of both the large and somewhat unpredictable amount of extinction at far-ultraviolet wavelengths (Bless and Savage 1972; York *et al.* 1973) and the desire not to waste *Copernicus* scanning time on stars too faint to provide reliable measurements, extensive use of OAO-2 broad-band photometry data (Code, Holm, and Bottemiller 1976) was made to select suitable program stars.

Our survey program has been restricted to column densities in the $J = 0$ and 1 rotational levels in order to obtain the total abundance of interstellar H_2 for a large sample of stars. A detailed examination of H_2 rotational populations toward a more limited sample of objects has already been undertaken by Spitzer, Cochran, and Hirschfeld (1974), who found that when $N(0)$ and $N(1)$ are greater than about 10^{17} cm^{-2}, less than 1% of the H_2 appears in levels with $J \geq 2$. The lines out of rotational levels $J = 2$ to 4 are often on the flat part of the curve of growth. To obtain column densities for these levels, many different lines must be observed and a curve of growth constructed. In contrast, for most of the stars of our investigation, the observed lines for the levels $J = 0$ and 1 have strong damping wings, and $N(0)$ and $N(1)$ can be determined in a straightforward manner by a profile-fitting process, assuming the lines are on the square-root part of the curve of growth.

b) *U1 Observations and Reductions*

An efficient observing routine was developed to obtain a U1 scan of the spectral region containing the $R(0)$, $R(1)$, and $P(1)$ lines in the H_2 (1, 0) Lyman band at 1092.19, 1092.73, and 1094.05 Å. Simultaneously, the U2 tube was used to scan the H I Lα line (see Paper II). The U1 tube has a resolution of 0.05 Å and steps in intervals of approximately 0.025 Å, and integrates for 14 s at each step position (Rogerson *et al.* 1973). The routine required about 3 hours of scanning time per star and was employed to observe the 52 stars denoted with comment 1 in column (17) of Table 1. The total number of counts recorded in the continuum near the H_2 lines in the 14 s integration time ranged from a low of 30 counts to a high of 4500. The statistical accuracy of the data obtained for the 30% of the stars which have net counts between 30 and 100 was improved by averaging twice over three adjacent channels, producing an effective resolution of about 0.1 Å. Owing to the open venting hole in the U1 phototube mount and to the simultaneous use of the U2 tube for the Lα study, part of the U1 data for the (1, 0) band contained stray light which entered through the venting hole (Rogerson *et al.* 1973), while the critical portion of the scan was obtained with the U2 mirror blocking the hole. An analysis demonstrated that the stray light was wavelength-independent from 1088 to 1096 Å. Particle backgrounds were supplied by the Princeton data-reduction programs. The zero level was established from the core of the strong H_2 lines. Wavelengths were shifted from the stellar reference frame to the interstellar frame by using the velocity of the most prominent interstellar cloud observed from the ground. The final zero point of the wavelength scale was established by locating, in the observed spectra, narrow H_2 lines for rotational levels with $J \geq 2$. The lines employed included one or more of the following: (2, 0) $P(4)$ 1088.79 Å, (1, 0) $R(2)$ 1094.24 Å, (2, 0) $R(5)$ 1089.51 Å, and (2, 0) $R(6)$ 1094.79 Å. This procedure assumes that the lines for levels with $J = 0$ and 1 have the same velocity as lines for levels with $J \geq 2$.

The final column densities were derived by a procedure similar to that employed previously to process Lα measurements (Jenkins 1971; Bohlin 1975). In this procedure, a reconstruction of the spectrum as it would appear in the absence of the H_2 (1, 0) $R(0)$, $R(1)$, and $P(1)$ lines was produced by dividing the observed spectrum by the quantity:

$$SF * \exp [\![-\{\tau_\lambda[R(0)] + \tau_\lambda[R(1)] + \tau_\lambda[P(1)]\}]\!] .$$

Where

$$\tau_\lambda[R(0)] = N(0)\frac{\pi e^2}{mc} f[R(0)]\phi_{R(0)}(\lambda - 1092.194) ,$$

$$\tau_\lambda[R(1)] = N(1)\frac{\pi e^2}{mc} f[R(1)]\phi_{R(1)}(\lambda - 1092.732) ,$$

$$\tau_\lambda[P(1)] = N(1)\frac{\pi e^2}{mc} f[P(1)]\phi_{P(1)}(\lambda - 1094.052) .$$

In these expressions, *SF*, the instrumental slit function, is convolved with the exponential function. *SF* was represented by a flat-topped Gaussian profile with full width at half-maximum (FWHM) = 0.051 Å (Drake *et al.* 1976). $\tau_\lambda[R(0)]$, $\tau_\lambda[R(1)]$, and $\tau_\lambda[P(1)]$ are the wavelength-dependent optical depths in the (1, 0) $R(0)$, $R(1)$, and $P(1)$ lines, respectively. The absorption oscillator strengths of Allison and Dalgarno (1970), $f[R(0)] = 0.00579$, $f[R(1)] = 0.00386$, and $f[P(1)] = 0.00193$, were used and are within 4% of the f-values tabulated by Morton and Dinerstein (1976). For the line shape functions $\phi_{R(0)}$, $\phi_{R(1)}$, and $\phi_{P(1)}$, Lorentzian profiles centered at each of the three

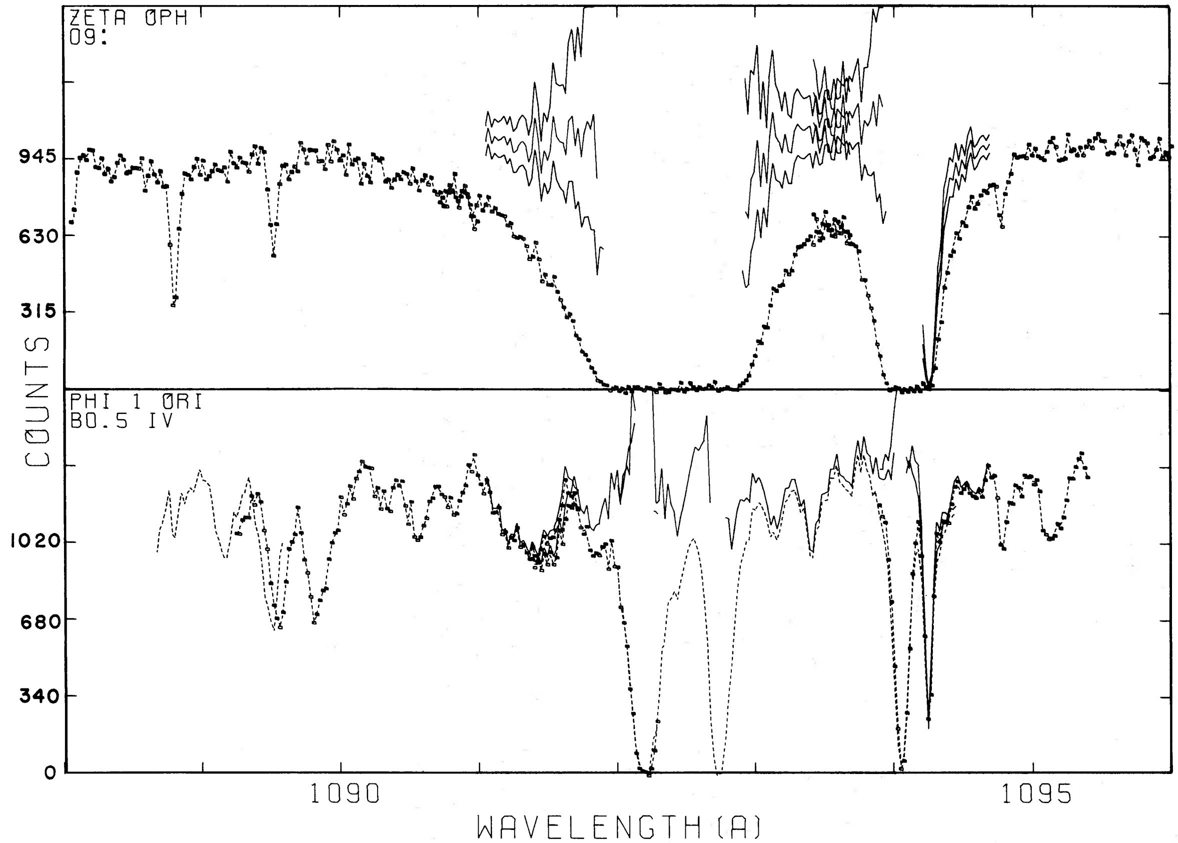

FIG. 1.—High-resolution (U1) scans of the H_2 (1, 0) Lyman lines for ζ Oph and ϕ^1 Ori corrected for stray and scattered light. For data obtained free of stray-light contamination, the data points are shown superposed on a dashed line. For data obtained with stray-light contamination, only a dashed line representing the observed spectrum is shown. The upper solid lines illustrate the reconstructed spectra for the strong $R(0)$, $R(1)$, and $P(1)$ lines at 1092.19, 1092.73, and 1094.05 Å. For ζ Oph the best fit is illustrated along with reconstructions for $N(0)$ and $N(1)$ values 20% larger and smaller. For ϕ^1 Ori, only the best-fit reconstruction is illustrated.

respective wavelengths were assumed. The damping constant, $\sum Aij$, is 1.741×10^9 s^{-1} for the (1, 0) band (Allison and Dalgarno 1970).

Different values of $N(0)$ and $N(1)$ were attempted until nearly complete cancellation of the strong interstellar lines was achieved. Near the line cores, where excessive magnification of small errors occurs, the reconstruction was not made. The values of $N(0)$ and $N(1)$ that gave the best reconstruction were taken as the final H_2 column densities unless the assumption of pure damping was invalid. Figures 1 and 2 illustrate reconstructions for four stars. The lower curve for each star represents the observed spectrum corrected to the interstellar H_2 wavelength frame. The upper curves are the reconstructed spectra. In the case of ζ Oph, three reconstructions are shown to demonstrate the effect that a 20% increase and a 20% decrease in $N(0)$ and $N(1)$ have over the best-fit values given in Table 1. For the other three stars, only the best-fit reconstructions are illustrated, although in the actual processing three reconstructions were made to permit an estimate of the uncertainty in the final column densities. The (1, 0) $R(2)$ 1094.24 Å line was not reconstructed, because it is not usually on the damping part of the curve of growth. In judging the best-fit reconstructions, one must make allowance for the presence of this line. Often the fitting procedure was confused by varying degrees of contamination arising from nearly stellar features, particularly for stars cooler than type B0.5. For these objects, unreddened comparison stars were used as a guide in selecting the best-fit reconstructions.

A key assumption in the reduction scheme outlined above is that the H_2 (1, 0) $R(0)$, $R(1)$, and $P(1)$ lines have pure damping profiles, i.e., the lines are formed on the square-root part of the curve of growth. In a number of cases the assumption breaks down. Table 2 was constructed to investigate the problem for the (1, 0) $R(0)$ line. The table contains the logarithmic error in $N(0)$ that would be made, if the actual profile were a Voigt profile with the effective velocity spread parameter, b, in km s^{-1}, instead of a damping profile. If the b-values are less than 10 km s^{-1}, Table 2 indicates that derived logarithmic column densities larger than about 19.0 should be accurate to 0.1 in the log. In contrast, if the b-values are as large as 20 km s^{-1}, a

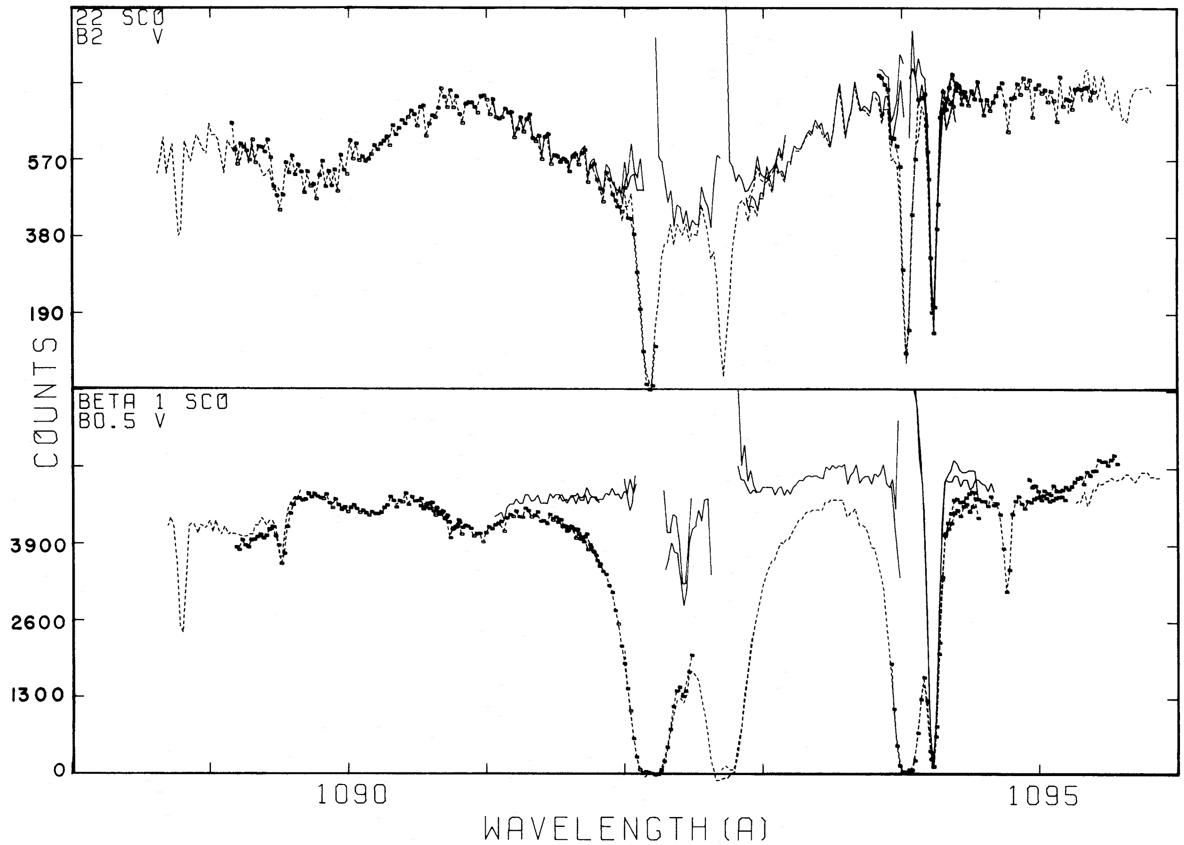

FIG. 2.—Same as Fig. 1 but for the stars 22 Sco and β^1 Sco. Only the best-fit reconstructions are shown.

logarithmic column density of 19.5 could have a logarithmic error of 0.18. In obtaining empirical curves of growth toward 28 stars, Spitzer, Cochran, and Hirschfeld (1974) found effective values of b ranging between 1.8 and 8.5 km s^{-1}. Unfortunately, the larger distances for some of the stars in the present investigation increase the probability of encountering multiple interstellar clouds and effective b-values in the range of 10 to 20 km s^{-1}. In most cases, the reconstructed profiles provide the information needed to confirm the validity of the reduction process. For example, ζ Oph and β^1 Sco in Figures 1 and 2 have H_2 (1, 0) $R(0)$, $R(1)$, and $P(1)$ lines with well-developed damping wings. For these two stars, the reconstruction is excellent for

TABLE 2

LOGARITHMIC DIFFERENCES BETWEEN PURE DAMPING AND VOIGT PROFILES

b (km s^{-1})	LOG $N(0)$				
	18.0	18.5	19.0	19.5	20.0
3............	0.07	0.01	0.00	0.00	0.00
6............	0.76	0.12	0.01	0.00	0.00
10............	2.06	0.72	0.10	0.01	0.00
20............	2.54	1.48	1.25	0.18	0.01
30............	2.62	1.74	1.48	0.78	0.10

both the $R(1)$ and $P(1)$ lines, even though the f-value of the $P(1)$ lines is one-half that of the $R(1)$ line. The best evidence for the breakdown of the pure damping assumption is usually obtained by comparing reconstructions for the $R(1)$ and $P(1)$ lines. Sometimes, the observed profiles are accurate enough to clearly show a non-Lorentzian shape. We have denoted those stars for which the damping profile assumption is invalid with a "D" in column (17) of Table 1 and report only approximate upper limits to $N(0)$ and $N(1)$ estimated from trial reconstructions. The true H_2 column densities for these stars will lie somewhere between ~0.002 and 1.0 times the number quoted, the smaller limit being determined by the assumption of no saturation. A more careful analysis could establish larger lower limits for most of these objects. However, owing to uncertainties in the zero level, the more careful method would yield results only a factor of 2 to 3 times larger. A full curve-of-growth analysis is planned for many of these stars when additional data are acquired.

c) U2 Observations and Reductions

Low-resolution spectral scans covering the wavelength interval 1040 to 1120 Å were available from the *Copernicus* U2 phototube for 34 stars. The resolution, step interval, and integration time were: 0.2 Å, 0.2 Å,

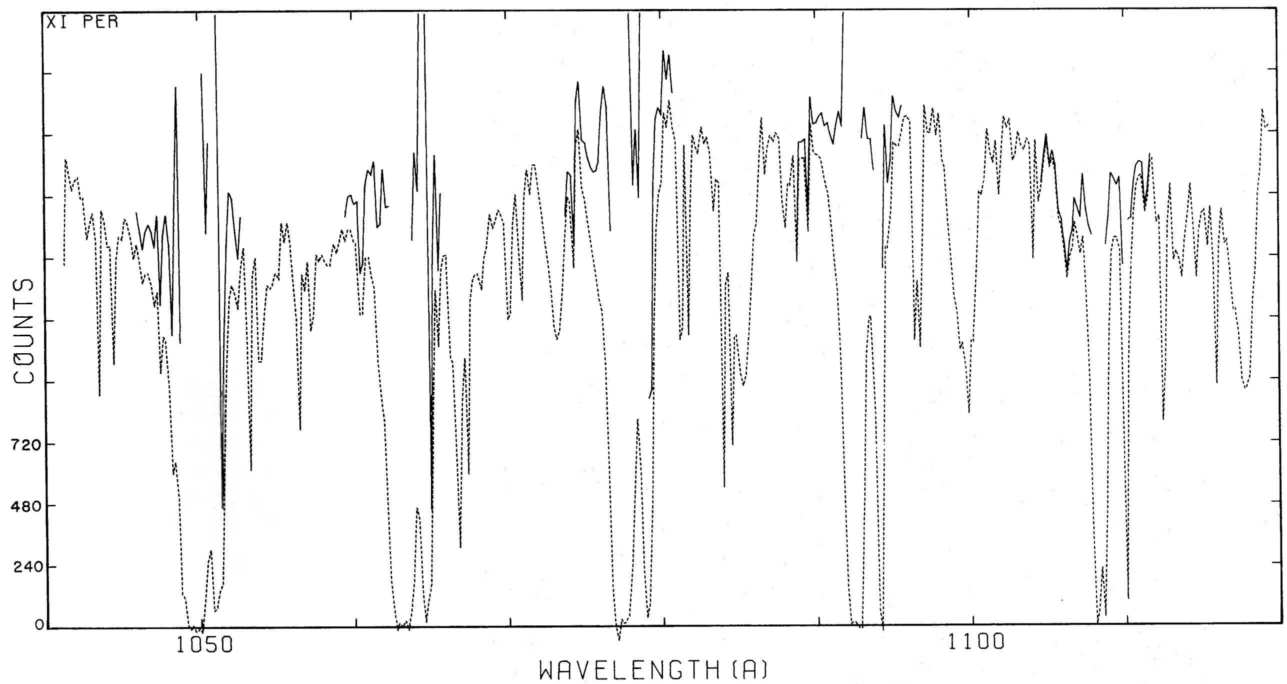

FIG. 3.—*Dashed line*, low-resolution (U2) scan of the H_2 (4, 0) to (0, 0) Lyman lines for the star ξ Per. *Upper solid line*, the best-fit reconstruction for the $R(0)$, $R(1)$, and $P(1)$ lines in each band.

and 14 s, respectively. These data provided 22 additional stars for which $N(0)$ and $N(1)$ could be derived and 12 for which it was possible to obtain only upper limits. The dashed line in Figure 3 illustrates a sample spectrum for ξ Per [O7.5 IIInf, $E(B-V) = 0.33$], a star with strong interstellar absorption in the (4, 0), (3, 0), (2, 0), (1, 0), and (0, 0) bands. See Table 1 in Morton and Dinerstein (1976) for precise wavelengths for the $R(0)$, $R(1)$, and $P(1)$ lines in each band.

Stray light and scattered light were removed from the original U2 spectra by using the reduction techniques described by Bohlin (1975). Further small adjustments to the zero level were then inferred from the cores of the strong H_2 lines. Measurements of the wavelengths of 27 sharp interstellar H_2 lines in the spectra of 17 stars demonstrated a need for corrections to the official U2 wavelength scale that ranged from 0.18 Å at 1025 Å to 0.04 Å at 1110 Å (Budich, Bohlin, and Drake 1976). For those stars exhibiting strong $R(0)$, $R(1)$, and $P(1)$ lines, we applied a continuum-reconstruction procedure identical to that used for the higher-resolution U1 spectra, except that the bands (4, 0) through (0, 0) were treated independently. Damping constants and f-values were again taken from Allison and Dalgarno (1970) but are in essential agreement with the more recent values tabulated by Morton and Dinerstein (1976). The U2 instrumental profile is a trapezoid with FWHM = 0.2 Å. The final values of $N(0)$ and $N(1)$ were determined from the best-fit reconstructions of all five bands. However, in many cases reconstructions of particular bands were ignored in the final averaging process because of stellar blending problems. The upper curve in Figure 3 illustrates, for ξ Per, the final reconstruction using the average best-fit values for $N(0)$ and $N(1)$. For the U2 spectra, the existence of data for lines differing in f-value by more than a factor of 10 provided confirmation that the lines in question were formed on the damping part of the curve of growth. The values of $N(0)$ and $N(1)$ given for 13 stars in Table 1 (identified in column [17] with comment "R") represent revisions over the values first quoted by Spitzer *et al.* (1973). The revised logarithmic column densities differ from the earlier values by amounts ranging from +0.22 to −0.68 in the log, although there is a general tendency for the new values to be smaller by about −0.2 in the log. A major part of the discrepancy between the preliminary and revised results may be explained by the fact that the stray-light and wavelength corrections were done with less precision in the earlier work. The significance of the stray-light problem can be judged from Figure 1 in Bohlin (1975). Also, we believe that the profile-fitting procedure described above provides a better way of judging the best-fit column densities than the scheme employed by Spitzer *et al.* (1973). For several objects, our more comprehensive analysis of line blending may explain the differences. For ζ Oph, σ Sco, and 10 Lac, U2 scans over the interval 1040 to 1120 Å exist, in addition to the high-resolution U1 data described in § II*b*. For all three stars, column densities derived from the two data sets are in excellent agreement with log difference <0.04. The U1 results are quoted in Table 1.

For a number of stars observed at low resolution, only upper limits to $N(0)$ and $N(1)$ are derivable. Most often these are relatively nearby stars for which H_2 lines are not detected, although in several cases H_2

lines are detected but severe blending or unfortunate positioning of the lines on the flat part of the curve of growth prevents a reliable determination of column densities. For these stars, upper limits to the equivalent widths for several of the $R(0)$, $R(1)$, and $P(1)$ lines were estimated. These upper limits range from 0.01 Å in stars with a good signal-to-noise ratio and smooth continua, to 0.1 Å in stars with numerous strong stellar features. For equivalent-width upper limits less than 0.02 Å, upper limits to $N(0)$ and $N(1)$ were derived by assuming the lines to be on the linear part of the curve of growth. For upper limits exceeding 0.02 Å, the column density upper limits were obtained with the conservative assumption that the lines are formed on the square-root part of the curve of growth. The final upper limits quoted in Table 1 for each star are for those lines that yield the smallest value for $N(0)$ and $N(1)$. The lines actually used to obtain the final estimates vary from object to object owing to the complex character of the stellar line blending.

d) *Errors*

Several categories of errors affect the results given in Table 1. First are the straightforward problems that influence the reliability of the plots of counts versus wavelength. These include the stray- and scattered-light corrections, the zero level correction, the wavelength correction, and the photon statistics. In all cases the photometric uncertainty owing to photon statistics in the averaged spectra is less than 10%. Second are those problems, difficult to assess reliably, that are the dominant source of error. These include contamination by stellar line blending and the curve-of-growth problems.

Column (10) of Table 1 gives the estimate of the logarithmic errors in the final values of $N(0)$ and $N(1)$, based on an estimate of the maximum likely contribution due to the above-mentioned problems. The major criterion used in estimating these errors was the character of the reconstructions for column densities larger and smaller than the best-fit values. Unreasonably large or small trial values of $N(0)$ and $N(1)$ produce reconstructions that obviously have improperly canceled line wings; for example, compare the three reconstructions for ζ Oph in Figure 1. The quoted logarithmic errors range from 0.06 to 0.28 and may be interpreted as representing approximately a 2 σ level of confidence. Errors due to stellar blending and curve-of-growth problems both act in the same sense, in that they tend to make the reported value larger than the true value. However, we have not listed asymmetrical errors to reflect this bias. Errors are not reported for the low column density objects for which only upper limits are derived.

e) *Explanation of Table 1*

The results of this investigation are listed in Table 1. For completeness, H_2 column densities from several earlier programs are also listed. The various columns contain the following information: (1) HD number; (2) name; (3) galactic longitude and (4) latitude (system II); (5) spectral type; (6) $E(B-V)$; (7) r, the distance in pc; (8) $\log N(0)$, where $N(0)$ is the H_2 column density in molecules cm^{-2} for the $J=0$ level; (9) $\log N(1)$, where $N(1)$ is the H_2 column density in molecules cm^{-2} for the $J=1$ level; (10) the logarithmic error in $N(0)$ and $N(1)$; (11) $\log N(H_2)$, where $N(H_2)$ is the total H_2 column density in molecules cm^{-2}; (12) $\log N(\text{H I})$, where $N(\text{H I})$ is the atomic hydrogen column density in atoms cm^{-2}; (13) $\log N(\text{H I} + H_2)$, where $N(\text{H I}+H_2) = N(\text{H I}) + 2N(H_2)$ is the total hydrogen column density in atoms cm^{-2}; (14) $\log f$, where $f = 2N(H_2)/N(\text{H I}+H_2)$; (15) T_{01}, the $J=0$ to 1 rotational temperature in K; (16) $n(\text{H I}+H_2) = N(\text{H I}+H_2)/r$, the average total hydrogen space density in atoms cm^{-3}; and (17) a comment column that indicates the source of the H_2 measurements according to the code given at the end of Table 1. An asterisk in column (17) implies that comments concerning the entries are given by HD number at the end of the table. The distances are calculated with the relation $m_V - M_V = 5\log r - 5 + 3E(B-V)$. Whenever possible, spectral types and absolute magnitudes are from Walborn (1971, 1972, or 1973) for the O stars and from Lesh (1968, 1972) for the B stars. The photometry used in obtaining r and $E(B-V)$ is usually from Lesh (1968, 1972) or otherwise from Blanco *et al.* (1970). Intrinsic colors are from Johnson (1966). For the Wolf-Rayet stars, absolute magnitudes are from Smith (1973*b*). The $E(B-V)$ values in parentheses are estimated from the photoelectric measurements of Stebbins, Huffer, and Whitford (1940).

$$N(H_2) = \sum_J N(J)$$

is assumed to be $N(0) + N(1)$ when $N(0) + N(1) \geq 10^{17}$ (see § II*a*). For $N(0) + N(1) < 10^{17}$,

$$\sum_J N(J)$$

is from Spitzer, Cochran, and Hirschfeld (1974) or York (1976). In obtaining the upper limits to $N(H_2)$ when $N(0) + N(1) < 10^{17}$, the procedures listed in the comments to Table 1 are followed. The atomic hydrogen column densities, column (12), are taken from Bohlin (1975) or Paper II, except for the θ^1 Ori C value, which is from Savage and Jenkins (1972).

III. DISCUSSION

The primary measurements of this investigation are the H_2 $J=0$ and 1 column densities, $N(0)$ and $N(1)$, listed in columns (8) and (9) of Table 1. Of these measurements, 70 are new results and 13 are revisions of preliminary results given by Spitzer *et al.* (1973); for completeness, 26 additional values have been taken from previous *Copernicus* publications.

a) *Object Distribution and Observational Selection*

The majority of the survey stars are located in O and B associations distributed along the galactic plane,

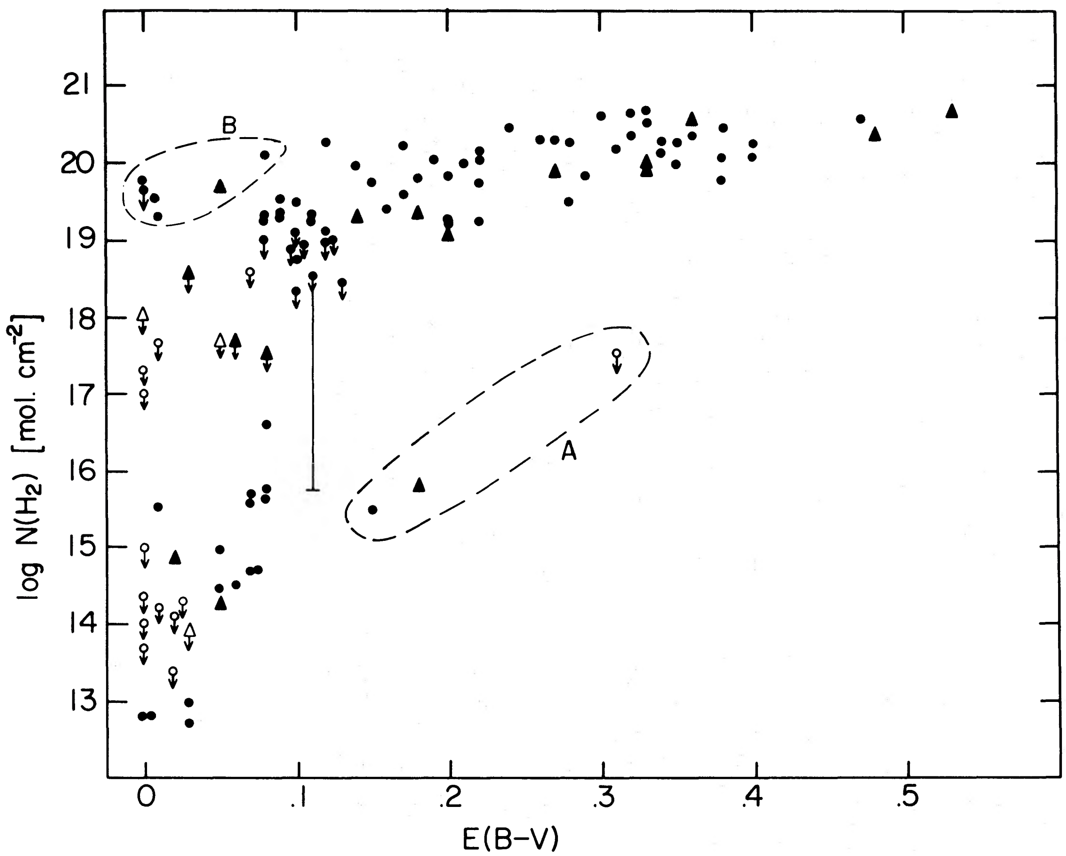

FIG. 4.—The logarithm of the total H_2 column density versus $E(B - V)$, a measure of the dust column density, for all the stars from Table 1. *Arrows on open symbols*, upper limits where H_2 is not detected. *Arrows on filled symbols*, upper limits where H_2 is detected but the damping profile assumption is invalid. In one case, the corresponding lower limit to $N(H_2)$ is also noted. Wolf-Rayet, Oe, Be, and peculiar stars are denoted with triangular symbols. Dashed regions, A and B, encircle discrepant points that are discussed in § III*c*.

although a few distant high-latitude stars were included to sample the gas well above the galactic plane (see § III*d*). The stars range in distance from 22 to 3400 pc, with the following number of stars in various distance intervals: $0 < r \leq 200$ pc, 33 stars; $200 < r \leq 500$ pc, 24 stars; $500 < r \leq 1000$ pc, 20 stars; $1000 < r \leq 2000$ pc, 24 stars; $r > 2000$ pc, eight stars. The survey is strongly biased toward stars within 1000 pc of the Sun. The stars have color excesses, $E(B - V)$, ranging from 0.00 to 0.53 with the following distribution: $0.00 \leq E(B - V) \leq 0.10$, 52 stars; $0.10 < E(B - V) \leq 0.20$, 22 stars; $0.20 < E(B - V) \leq 0.30$, 13 stars; $0.30 < E(B - V) \leq 0.40$, 19 stars; and $E(B - V) > 0.40$, three stars. For the 109 stars, the overall average for $\sum E(B - V)/\sum r$ is 0.22 mag kpc^{-1}. Since the local average for matter in the plane within 1000 pc of the Sun is 0.61 mag kpc^{-1} (Spitzer 1968), the survey is biased toward stars with less than normal reddening per unit distance. For additional discussions of the sampling biases of ultraviolet interstellar surveys, see Jenkins and Savage (1974), Jenkins (1976), and Paper II.

b) *Correlations*

Figures 4, 5, and 6 were prepared to investigate how

$$N(H_2) = \sum_J N(J)$$

and $f = 2N(H_2)/[N(\text{H I}) + 2N(H_2)]$ depend on $E(B - V)$ and $N(\text{H I} + H_2) = N(\text{H I}) + 2N(H_2)$. The measurements for peculiar, Oe, Be, and Wolf-Rayet stars are plotted as triangles. The arrows attached to open symbols denote cases where H_2 was not detected but an upper limit is quoted. The arrows attached to filled symbols imply that H_2 was detected but, owing to curve-of-growth uncertainties, we quote only an upper limit. In the latter instance, an approximate lower limit to $N(H_2)$ would lie a factor of 500 below the point plotted (see § II*b*). For one case (23 Ori), a vertical line denotes the lower limit.

Figure 4 shows log $N(H_2)$ versus $E(B - V)$. With the exception of the points enclosed within the two dashed regions (to be discussed in § III*c*), log $N(H_2)$ undergoes a sharp transition from small values to large

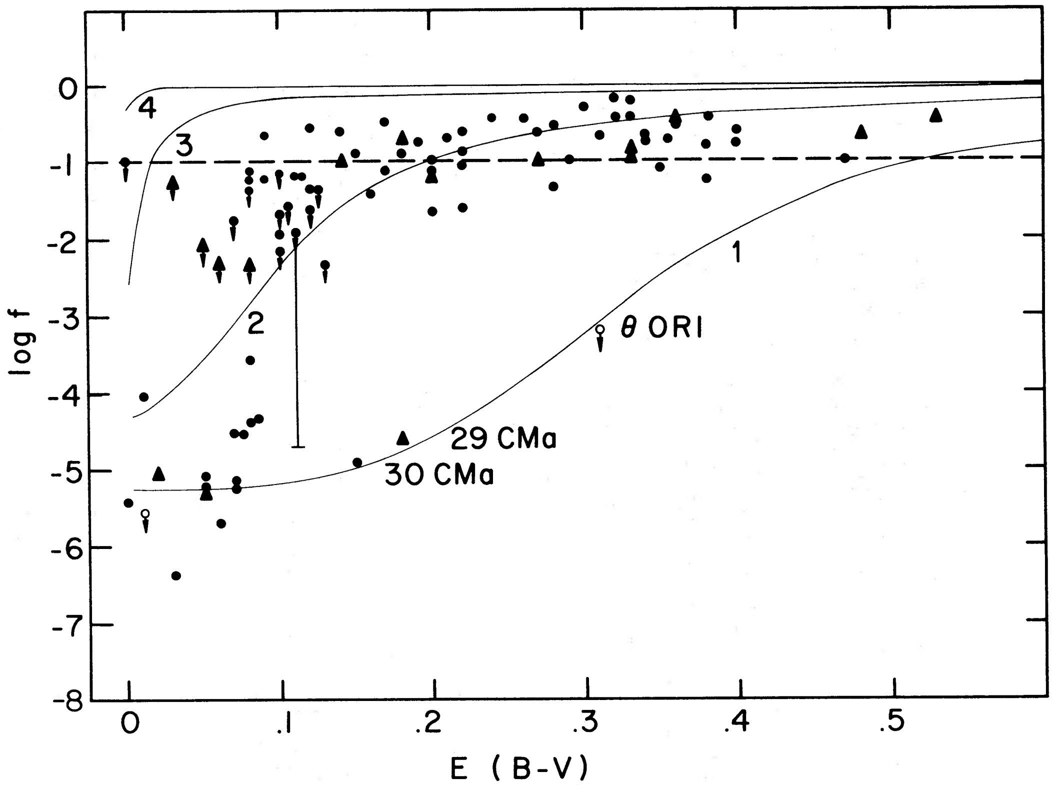

FIG. 5.—The logarithm of f, the fractional abundance of H_2, versus $E(B-V)$. See legend of Fig. 4 for a discussion of the different symbols. A dashed line divides the plot into regions with $f > 0.1$ and $f < 0.1$. This figure contains fewer points than Fig. 4, since N(H I) cannot be measured for all the survey stars. The four thin solid lines are Black's equilibrium calculations for the parameter values listed in Table 5.

values at $E(B-V) \approx 0.08$. Over the range $E(B-V) \approx 0.15$ to 0.5, $\log N(H_2)$ steadily increases from an average of approximately 19.5 to 20.5. For $E(B-V) \geqslant 0.10$, the values of $N(H_2)$ have a peak-to-peak spread amounting to about a factor of 10. In reviewing the results for a smaller sample of *Copernicus* H_2 measurements, Spitzer and Jenkins (1975) called attention to a pronounced void of column densities in the range $17 < \log N(H_2) < 19$. Unfortunately this void represents a range of column densities where the new measurements have curve-of-growth uncertainties; and, generally, only upper limits are quoted in Table 1. An inspection of Figure 4 reveals that 18 stars have upper limits falling in the region, $17 \leq \log N(H_2) \leq 19$, and one actual measurement falls in this zone. The existence of a void region in Figure 4 will depend on how far below the quoted upper limits the true $N(H_2)$ measures lie for the 18 stars. The upper limits denoted with filled symbols have a lower limit to $N(H_2) \sim 500$ times smaller than the value plotted. Unfortunately, the large spacing between these upper and lower limits spans the region of interest. A full curve-of-growth analysis must be undertaken for a number of the upper limit points to resolve the question of whether or not the void region actually exists.

Figure 5 shows $\log f$, the fractional abundance of hydrogen in the molecular form, plotted versus $E(B-V)$ for 91 stars. The general characteristics of this figure and Figure 4 are similar, although the points from region B Figure 4 are missing owing to a lack of H I column densities for these stars. The measured values of f range from a low of 4.2×10^{-7} for λ Sco (York 1976) to a high of 0.63 for ζ Oph. The horizontal dashed line divides Figure 5 into regions with f greater than and less than 0.1. For $E(B-V) < 0.15$, 88% of the stars observed have $f < 0.1$, while for $E(B-V) \geq 0.15$, 74% have $f \geq 0.1$. Ignoring upper limit measurements, peculiar, Oe, Be, and Wolf-Rayet stars, and stars with uncertain photometry, we find the following average values of

$$\langle f \rangle = \sum 2N(H_2) \Big/ \Big[\sum N(\text{H I} + H_2)\Big]$$

for the various $E(B-V)$ intervals: $0 \leq E(B-V) \leq 0.1$, $\langle f \rangle = 0.019$, 18 stars; $0.1 < E(B-V) \leq 0.2$, $\langle f \rangle = 0.12$, 15 stars; $0.2 < E(B-V) \leq 0.3$, $\langle f \rangle = 0.21$, 12 stars; and $0.3 < E(B-V) \leq 0.53$, $\langle f \rangle = 0.22$, 18 stars. The slow increase in f with $E(B-V)$, for $E(B-V) > 0.15$, is evident in the figure and in these averages.

Figure 6 is a plot of $\log f$ versus $N(\text{H I} + H_2)$. Figures 5 and 6 are roughly similar in appearance, although the correlation of f with $E(B-V)$ is somewhat better than with $N(\text{H I} + H_2)$. In Figure 6 the transition from small f to large f occurs at about $N(\text{H I} + H_2) \approx 5 \times 10^{20}$ atoms cm^{-2}. Differences

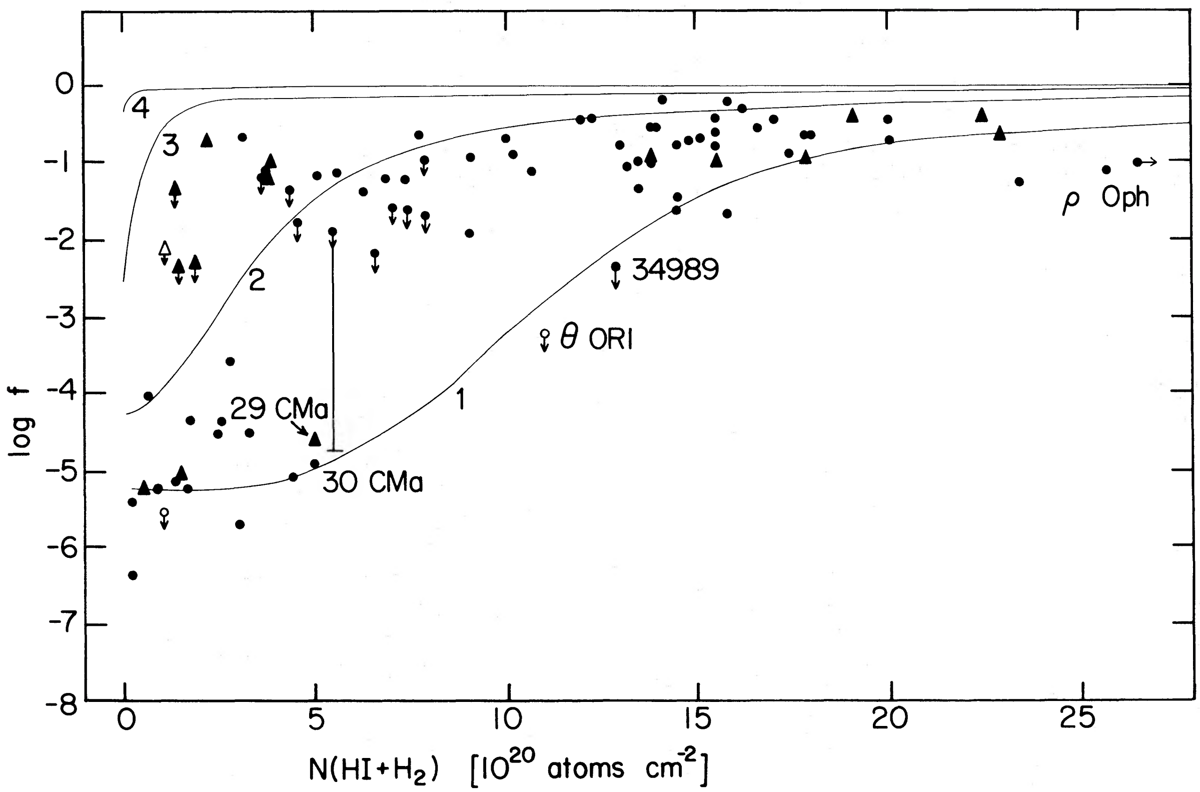

FIG. 6.—A plot of $\log f$ versus the total gas column density, $N(\text{H I} + \text{H}_2) = N(\text{H I}) + 2N(\text{H}_2)$. See legend of Fig. 4 for a discussion of the different symbols. The point for ρ Oph should be moved off the graph to $N(\text{H I} + \text{H}_2) = 72 \times 10^{20}$ atoms cm^{-2}. The four thin solid lines are Black's equilibrium calculations for the parameter values listed in Table 5.

between Figures 5 and 6 can be understood by referring to Figure 7, which shows $\log f$ versus the gas-to-color-excess ratio, $N(\text{H I} + \text{H}_2)/E(B - V)$, for all stars with $E(B - V) \geq 0.1$. The symbol coding is the same as for Figures 4, 5, and 6. The dashed vertical line denotes the average ratio, 5.9×10^{21} atoms cm^{-2} mag^{-1}, from Paper II. Although there are some exceptions (29 and 30 CMa, θ Ori), in general, objects with $\log f < -1.4$ have a larger than normal gas-to-dust ratio implying either an excess of gas or deficiency of dust. The trend exhibited in Figure 7 can perhaps be taken as observational evidence that the presence of dust favors H_2 formation. However, such trends can often occur for indirect reasons or through a sampling bias.

c) *Stars with Abnormally Small or Large* $N(\text{H}_2)$

The data points of Figure 4 enclosed in the dashed regions represent objects for which the H_2 column densities are either abnormally small (region A) or abnormally large (region B) when compared with the trends exhibited by the majority of the stars. The stars in region A are θ^1 Ori C, 29 CMa, and 30 CMa. The small values of $N(\text{H}_2)$ toward 29 and 30 CMa may be related to the fact that both stars lie in the galactic sector from $l^{\text{II}} = 220°$ to $280°$, a region having a very low average space density of atomic hydrogen (see Paper II and Bohlin 1975). However, in Figure 6 the data points for these objects are less discrepant, possibly implying that $E(B - V)$ is overestimated for these two luminous O-type stars. The small upper limit of $N(\text{H}_2)$ toward θ^1 Ori C is peculiar for a star with $E(B - V) = 0.31$. The OAO-2 Lα measurement for θ^1 and θ^2 Ori (Savage and Jenkins 1972) of $\log N(\text{H I}) = 21.04$ indicates that an extensive neutral hydrogen cloud probably exists along the line of sight to θ^1 Ori C. A larger than normal flux of dissociating radiation may explain the small upper limit for $N(\text{H}_2)$. An alternative possibility is the abnormal nature of the interstellar dust in the Orion region. The extinction characteristics of the dust are peculiar in both the infrared (Johnson 1968) and ultraviolet (Bless and Savage 1972). The ratio of total to selective extinction is larger than normal, the usual far-ultraviolet rise in extinction near 1300 Å is absent, and the ubiquitous 2200 Å bump is very weak. These measurements suggest an absence of small interstellar grains which could be the H_2 formation sites. To explore this possibility further we investigated the correlation between $N(\text{H}_2)$ and various ultraviolet indicators of extinction. If H_2 preferentially forms on the small grains producing the ultraviolet extinction, we might expect such correlations as $N(\text{H}_2)$ versus $E(1300 - V)$ or $N(\text{H}_2)$ versus $E(\text{bump})$ to show less scatter than the $N(\text{H}_2)$ versus $E(B - V)$ correlation. Here $E(1300 - V)$ refers to the excess between 1300 Å and the photoelectric V band, while $E(\text{bump})$ is a measure of the

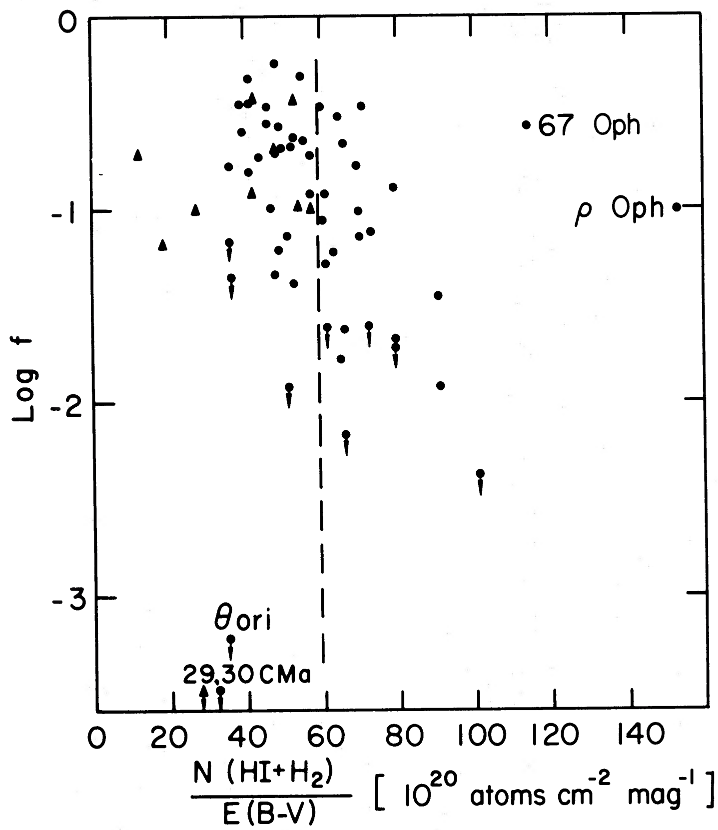

FIG. 7.—Log f versus $N(\mathrm{H\ I} + H_2)/E(B-V)$, the gas-to-color-excess ratio, for stars with $E(B-V) \geq 0.1$. The vertical dashed line denotes the mean gas-to-color-excess ratio from Paper II. The data points for 29 and 30 CMa should be moved off the bottom of the graph to log $f = -4.62$ and -4.92, respectively. Wolf-Rayet, Oe, Be, and peculiar stars are denoted with triangular symbols.

extinction in the 2200 Å feature. Values for these ultraviolet measures of extinction for 36 of the H_2 survey stars were taken from the OAO-2 broad-band extinction measurements of Code and Cashdollar (private communication). Unfortunately, the result was inconclusive, since correlations of $N(H_2)$ with the visual and ultraviolet indicators of extinction exhibited approximately the same amount of scatter. Apparently the variation in $N(H_2)$ for a given $E(B-V)$ exhibited in Figure 4 is at most only slightly influenced by changes in the dust characteristics toward each star. These correlations did not include 29 and 30 CMa, since ultraviolet extinction measurements have not been reported for these two stars.

The stars in region B (ignoring the upper limit point) that have abnormally large H_2 column densities for the corresponding $E(B-V)$ include: δ Per, 20 Tau, 23 Tau, η Tau, and ο And. These are all relatively nearby stars with spectral types ranging from B5 to B8. The extinction characteristics of the dust toward some of these stars in the ultraviolet can be inferred from the OAO-2 photometric data of Code *et al.* (1976) and Code and Meade (1976). In all cases, the ultraviolet measurements are consistent with a small amount of normal interstellar reddening. Adams (1949) noted that a number of stars in the Pleiades have abnormally strong CH^+ lines (see notes to Table 1) and suggested a circumstellar origin for this molecule. More recently, Hobbs (1972, 1973) has rediscussed the circumstellar origin of CH^+ toward 20 and 23 Tau. Perhaps the mechanism that produces the abnormal CH^+ can also explain the large H_2 column densities observed toward these stars. The presence of H_2 and CH^+ and the absence of CH and CN toward some of these stars may provide important clues about interstellar molecule formation. The one common property exhibited by the stars in region B is their spectral type range, from B5 to B8. Perhaps the deficiency of dissociating ultraviolet flux in the 912 to 1108 Å region permits the survival of H_2 molecules in the vicinity of such stars. The *Copernicus* far-ultraviolet data indicate that unreddened B0 and B7 stars which have the same visual magnitude differ in flux at 1100 Å by about a factor of 70.

d) *High-Latitude Stars*

In order to study atomic and molecular hydrogen well above the galactic plane, we observed a number of distant stars at high galactic latitudes. Table 3 summarizes the H_2 measurements for these stars, where z is the distance above the galactic plane. The table includes two stars (HD 28497 and HD 91316) from previous *Copernicus* papers. In all cases, the

TABLE 3

DISTANT HIGH-LATITUDE STARS

HD	b^{II}	r (pc)	z (pc)	log N(H I)	log $N(H_2)$	log f
28497.........	−37	466	280	20.20	14.82*	−5.08
91316.........	+53	959	766	20.26	15.61†	−4.35
93521.........	+62	1778	1570	20.11	< 18.54	< −1.27
149881.........	+36	1614	949	20.65	< 19.00	< −1.35
210191.........	−52	336	265	< 20.66	< 18.60	...
214080.........	−57	3404	2855	20.64	< 19.00	< −1.34
219188.........	−50	2355	1804	20.85	19.34	−1.23

* $N(H_2)$ from York 1976.

† $N(H_2)$ from Spitzer *et al.* 1974.

value of f is small. Care must be taken in interpreting these numbers, because much of the H_2 and H I absorption may be produced by local gas ($z < 200$ pc). The star HD 93521 is of particular interest, since the absorptions for the local and high z gas have a large velocity separation. Table 4 summarizes the velocity structure of the interstellar line spectrum of HD 93521. The entries for Ca II and Na I were taken from Münch and Zirin (1961) and Cohen (1974). The 21 cm H I data were taken from Habing (1969*a*, *b*). Paper II discusses the 21 cm–Lα comparison for this star. Münch and Zirin (1961), Habing (1969*a*, *b*), and Rickard (1972) have provided evidence that the gas components at -56 and -34 km s^{-1} are due to gas at $z \gtrsim 500$ pc. In the *Copernicus* U1 spectrum for this star, the strong H_2 (1, 0) $R(0)$, $R(1)$, and $P(1)$ lines have $V_{\text{heliocentric}} = -2.2 \pm 10$ km s^{-1}. These lines probably originate in the cloud at -12 km s^{-1}, although the observed absorptions may be formed in both the -12 and $+5$ km s^{-1} clouds. In either case, there is no evidence for $J = 0$ or 1 H_2 absorption at either -56 or -34 km s^{-1} with an equivalent-width upper limit of 20 mÅ. The H_2 upper limits for these clouds in Table 4 were obtained with the assumption that lines as weak as 20 mÅ would be on the linear portion of the curve of growth. A rotational temperature of 1000 K was assumed to obtain a conservative upper limit on

$$N(H_2) = \sum_J N(J)$$

from $N(0) + N(1)$. Using the 21 cm column density for the cloud at -56 km s^{-1}, we obtain $f < 1.6 \times 10^{-4}$ for this particular high z cloud. In conclusion, there is no evidence in these data for the existence of appreciable amounts of H_2 in the halo gas.

e) Comparison with Theories of H_2 *Formation and Destruction*

Van de Hulst (1948) first suggested that interstellar H_2 might form on the surface of interstellar grains, and Stecher and Williams (1967) first discussed the two-step photodissociation process that probably destroys H_2 in H I regions. In recent years, a number of investigators have calculated in detail the expected *equilibrium* abundance of interstellar H_2 (Hollenbach, Werner, and Salpeter 1971; Glassgold and Langer 1973; Jura 1975*a*, *b*; Black 1975; for a brief review, see Spitzer and Jenkins 1975). To compare the observations with the *equilibrium* theory, model calculations were kindly supplied by J. Black (private communication). The calculations are described in Black (1975, Chap. 4). The radiative transfer in the photodissociating lines was accurately modeled. Less accurate transfer calculations, such as those employed by Hollenbach, Werner, and Salpeter (1971) and Glassgold and Langer (1974), underestimate the H_2 photodissociation rate in the transition region from small to large H_2 column densities by about a factor of 10 (Black, private communication). The primary free parameters are: (1) I(1000 Å) (ergs cm^{-3} Å^{-1}), the density of 1000 Å radiation at the cloud boundary; (2) R(cm^3 s^{-1}), a measure of the formation efficiency of H_2 on grain surfaces, where the formation rate is $Rn(\text{H I})n(\text{H I} + H_2)$ (molecules cm^{-3} s^{-1}); (3) the values of total density, $n(\text{H I} + H_2)$; (4) the temperature at each position in the cloud; (5) δV, the velocity width of the H_2 lines, where $\delta V = 1.665b$; and (6) the

TABLE 4

INTERSTELLAR COMPONENTS FOR HD 93521

$V_{\text{heliocentric}}$ (km s^{-1})	log N(Ca II)* (cm^{-2})	log N(Na I)* (cm^{-2})	log N(H I)† (cm^{-2})	log $N(H_2)$ (cm^{-2})
−56............	11.8	...	19.3	< 15.2
−34............	11.3	11.0	...	< 15.2
−12............	12.2	12.4	19.9	< 18.54
+5.............	11.5	...	...	...

* From Cohen 1974.

† 21 cm column densities from Habing 1969*a*.

TABLE 5

BLACK'S MODEL PARAMETERS

Model	$n(\text{H I} + \text{H}_2)$ (cm^{-3})	T (K)	I(1000 Å) (10^{-17} ergs cm^{-3} Å^{-1})	R (10^{-17} cm^3 s^{-1})
1.............	10	100	4.0	1.0
2.............	100	100	4.0	1.0
3.............	1000	100	4.0	3.0
4.............	10000	20	4.0	3.0

cloud thickness, measured in $E(B - V)$ or $N(\text{H I} + \text{H}_2)$. The calculations are for plane-parallel clouds, and the derived quantities are the column densities of various species through the clouds. The models assume constant temperature and total density. Comparisons between the observations and Black's theory are shown in Figures 5 and 6. The model curves illustrated by the solid lines numbered 1 through 4 were derived for the parameter values listed in Table 5. Along each model curve, the cloud thickness varies. The value of the radiation field is representative of the mean interstellar background field. The values of R assume efficient conversion of atomic to molecular hydrogen on grain surfaces. In all four models, $\delta V = 5.0 \text{ km s}^{-1}$. For the assumed values of I(1000 Å) and R, Black's model densities in the range of ~ 10 to $\sim 500 \text{ cm}^{-3}$ appear to adequately describe the trends exhibited by the data. Measurements that deviate significantly from the general trends could be explained by excessively large or small values of $n(\text{H I} + \text{H}_2)$. However, large changes in I(1000 Å) and/or R may be required in certain cases. For example, the point for ρ Oph in Figure 6 [$\log f = -1.0$, $N(\text{H I} + \text{H}_2) = 7.2 \times 10^{21} \text{ cm}^{-2}$] may require a large value of I and/or a small value of R.

A *nonequilibrium* theory involving H_2 formation in a shell of swept-up matter surrounding O and B stars that have stellar winds has recently been proposed by Hollenbach, Chu, and McCray (1976). In this theory the formation of molecules on grains is not in equilibrium with photodestruction. The theory explains a number of H_2 observations in a natural way. The most straightforward way of establishing the validity of the nonequilibrium theory is through precision velocity correlations of the H_2 lines and other circumstellar shell lines. The recent H_2 velocity measurements of Spitzer and Morton (1976) provide support for the nonequilibrium theory for some stars.

In summary, recent equilibrium calculations adequately describe many of the H I and H_2 measurements presented in this paper. However, for some stars, more complex nonequilibrium phenomena may govern the formation of and/or destruction of H_2.

f) The 0–1 *Rotational Temperature*

The $J = 0$ to 1 H_2 rotational temperature as obtained from the expression,

$$\frac{N(1)}{N(0)} = \frac{g_1}{g_0} \exp(-E_{01}/kT_{01}) = 9 \exp(-170[\text{K}]/T_{01}),$$

is given in column (15) of Table 1. For clouds with strong self-shielding [$N(0)$ and $N(1) > 10^{17} \text{ cm}^{-2}$], collisions of molecules with protons should outweigh other processes in determining the relative population of the $J = 0$ and 1 levels (Dalgarno, Black, and Weisheit 1973). Therefore, the $J = 0$ to 1 population ratio is a measure of the proton kinetic temperature and, hence, cloud kinetic temperature. For clouds which do not have strong self-shielding, radiative processes will probably dominate the collisional processes in establishing the $J = 0$ to 1 population ratio (Jura 1975*a*, *b*). Since most of the new observations are for stars with strong self-shielding, we will restrict the discussion to these cases.

T_{01} has been measured toward 61 stars having $N(0)$ and $N(1)$ larger than 10^{18} cm^{-2}. The values range from 45 K for λ Ori to 128 K for HD 53975. For the 61 stars we find the average,

$$\langle T_{01} \rangle = 77 \pm 17 \text{ (rms) K}.$$

This number is in agreement with the earlier *Copernicus* results of Spitzer and Cochran (1973) for 13 stars. A comparison of 21 cm emission and absorption measurements provides an independent method of obtaining the cloud kinetic temperature. From high-resolution 21 cm studies, Hughes, Thompson, and Colvin (1971) and Radhakrishnan *et al.* (1972) report temperatures ranging from 15 to 250 K with a mean temperature of 60 to 80 K, in agreement with the 77 K mean found from H_2 absorption.

The heating and cooling processes that influence the cloud kinetic temperature are still only poorly understood (Dalgarno and McCray 1972). In the hope that the measurements of Table 1 could provide new insights about the thermal properties of clouds, we investigated various correlations between T_{01} and cloud parameters. No correlation is found between T_{01} and the following quantities: f, $[N(\text{H I}) + 2N(\text{H}_2)]/E(B - V)$, $E(B - V)$, $N(\text{H I})$, and $[N(\text{H I}) + 2N(\text{H}_2)]$. However, weak correlations exist between T_{01} and the following: $N(\text{H}_2)$, $E(B - V)/r$, $n(\text{H}_2)$, and $n(\text{H I} + \text{H}_2) = [N(\text{H I}) + 2N(\text{H}_2)]/r$. The sense of these correlations is that T_{01} decreases for larger values of $N(\text{H}_2)$, $E(B - V)/r$, $n(\text{H}_2)$, and $n(\text{H I} + \text{H}_2)$. Figure 8 illustrates the T_{01} versus $n(\text{H I} + \text{H}_2)$ correlation. The trend exhibited by the entire sample of stars is also observed for stars in selected regions. For example, note the trend for stars in the Scorpius-Ophiuchus region which have been denoted with squares in Figure 8. Ignoring the problems associated with sampling biases and the fact that multiple clouds are encountered for most lines of sight, we believe that

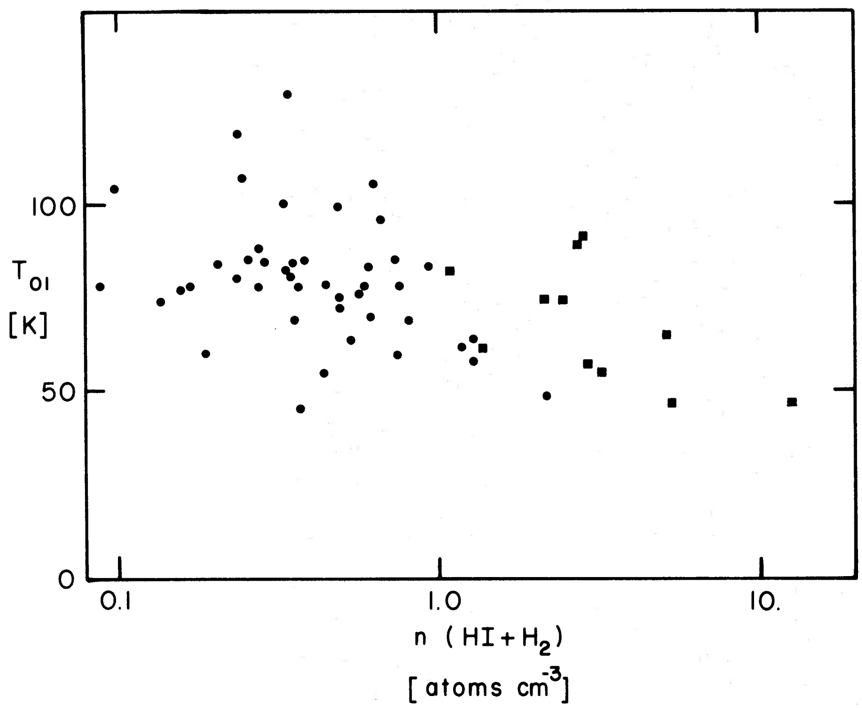

FIG. 8.—The correlation between the $J = 0$ to 1 rotational temperature and $n(\text{H I} + \text{H}_2) = [N(\text{H I}) + 2N(\text{H}_2)]/r$, a crude indicator of density. The stars plotted all have $N(0)$ and $N(1) > 10^{18}$ molecules cm^{-2}. Stars in the Scorpius-Ophiuchus region are denoted with squares. The plot possibly implies that T_{01} is lower in denser clouds. The correlation between T_{01} and $E(B - V)/r$ is similar to this figure.

the various correlations suggest that: (1) changes in the gas-to-dust ratio by a factor of 3 and changes in f by a factor of 10 have negligible effects on cloud temperatures; (2) the thickness of a diffuse cloud as measured by $E(B - V)$ or $N(\text{H I} + \text{H}_2)$ does not influence its temperature, although the total column density of H_2 through the cloud does have an effect; and (3) the denser clouds are cooler, assuming that $E(B - V)/r$, $n(\text{H}_2)$, and $n(\text{H I} + \text{H}_2)$ are crude indicators of the relative densities within clouds.

g) The Average H_2 *Abundance in the Solar Neighborhood*

For 76 stars having measures of $N(\text{H}_2)$ and $N(\text{H I})$ and reliable values for $E(B - V)$, (i.e., excluding Wolf-Rayet, Oe, Be, and peculiar stars, and stars with uncertain photometry), the following overall averages result: $\langle n(\text{H}_2)\rangle = \sum N(\text{H}_2)/\sum r = 0.036$ molecules cm^{-3}, $\langle n(\text{H I})\rangle = \sum N(\text{H I})/\sum r = 0.35$ atoms cm^{-3}, $\langle f\rangle = 2\langle n(\text{H}_2)\rangle/[2\langle n(\text{H}_2)\rangle + \langle n(\text{H I})\rangle] = 0.17$, $\sum E(B-V)/\sum r = 0.22$ mag kpc^{-1}, $\langle E(B - V)\rangle = 0.17$ mag, and $\langle r\rangle = 0.76$ kpc. Owing to observational bias against observing highly reddened stars, these numbers have no fundamental significance but only indicate representative results one finds when observing bright early-type stars. To obtain the actual average that applies within the solar neighborhood, sampling biases must be accounted for. The average results above are for lines of sight for which the average reddening per unit distance is less than the local average of $\langle E(B - V)/r\rangle = 0.61$ mag kpc^{-1} (Spitzer 1968) that applies to matter in the plane within 1000 pc of the Sun. Since the equilibrium abundance of H_2 increases with density, and the observations sample stars with below average density, the local average of $n(\text{H}_2)$ and f for matter in the galactic plane must be greater than the averages obtained above for the survey stars. Jenkins (1976), in analyzing a preliminary version of Table 1, made a plot of $n(\text{H}_2)$ versus $E(B - V)/r$ for all the survey stars and assumed that $\langle n(\text{H}_2)\rangle$ and $\langle f\rangle$ could be roughly estimated from those data points having the average local reddening per unit distance. Unfortunately the result, $\langle f\rangle \approx 0.2$, was very uncertain owing to a large amount of scatter in the plot for $E(B - V)/r \geqslant 0.5$ mag kpc^{-1}. A better procedure relies on the fact that observationally, $N(\text{H}_2)$ and $E(B - V)$ are reasonably well correlated (see Fig. 4), even though the survey stars have a large range in distance for a given $E(B - V)$. To exploit this correlation, the galactic extinction distribution measurements of FitzGerald (1968) have been used. For each 10° zone along the plane of the Galaxy, an average $E(B - V)$ was determined from FitzGerald's Figure 5, which is a plot of extinction as a function of l^{II} and b^{II} for stars at a distance of 500 pc. From these measurements an average reddening in the plane of 0.62 mag kpc^{-1} is obtained, a result in agreement with the average quoted by Spitzer (1968). Therefore the distance of 500 pc is large enough to obtain representative local averages for interstellar quantities. Averages over smaller distances would be significantly influenced by the region of low gas density in the immediate vicinity of the Sun (Jenkins and Savage 1974; Bohlin 1975). For a distance of 1000 pc, we could not take full advantage of the empirical relation between $N(H_2)$ and $E(B-V)$ found in Figure 4 because many directions have color excesses exceeding 0.6 mag. In addition, sampling biases appear to strongly influence extinction data for stars more distant than 500 pc. From the average $E(B-V)$ for each 10° zone, an average $N(H_2)$ was read from a mean line through the data points in the log $N(H_2)$ versus $E(B-V)$ plot. For two zones, it was necessary to extrapolate the observed relation to excesses between 0.7 and 0.9. An average of the 36 individual values of $N(H_2)$ yielded $\langle N(H_2)\rangle = 2.2 \times 10^{20}$ molcules cm^{-2}, which implies $\langle n(H_2)\rangle = 0.143$ molecules cm^{-3}. Combining this with the estimate of $\langle n(\text{H I} + H_2)\rangle =$ 1.15 atoms cm^{-3} from Paper II, we conclude $\langle n(\text{H I})\rangle = 0.86$ atoms cm^{-3} and $\langle f\rangle = 0.25$. These averages apply to matter in the galactic plane within 500 pc of the Sun. The true value of $\langle f\rangle$ may be larger, for the following reasons: (1) the procedure for calculating $\langle N(H_2)\rangle$ does not properly allow for a dispersion in $E(B-V)$ within each 10° zone; (2) there may be observational bias against highly obscured stars closer than 500 pc in the work of FitzGerald (1968); (3) the stars used to define the log $N(H_2)$ versus $E(B-V)$ relation have average distances considerably larger than 500 pc; and (4) the survey stars are mostly hot stars that have large fluxes of dissociating ultraviolet radiation. Because of all these problems, the estimates for $\langle n(H_2)\rangle$ and $\langle f\rangle$ should be considered lower limits.

IV. CONCLUDING REMARKS

The entries of Table 1 provide basic reference data for studies of the local interstellar material. For example, regional variations in elemental depletions could be measured by obtaining heavy-element column densities toward a subset of the stars for which $N(\text{H I} + H_2)$ now exists. Such investigations are being pursued in the optical for Ti II (Stokes and Hobbs 1976) and in the ultraviolet for Fe II (Savage and Bohlin 1977), and for a sample of heavy elements through a new *Copernicus* interstellar abundance survey (York, private communication). It will be interesting to see how variations in the depletion relate to variations in cloud parameters. Accurate column densities for such molecules as CH, CH^+, CN, CO, and HD are needed toward a group of the H_2 survey stars. Intercomparisons of these column densities with $N(\text{H I})$ and $N(H_2)$ may provide clues about the chemical processing occurring within diffuse clouds and circumstellar shells. The largest body of reliable data exists for CH^+ (Hobbs 1973) and CO (Jenkins 1976; Jenkins and Shaya 1977). Correlations between $N(CH^+)$ and $N(H_2)$, $N(\text{H I} + H_2)$ and $E(B-V)$ for 15 stars measured by Hobbs (1973) all exhibit a large amount of scatter. The CH^+/H_2 column density ratio ranges from 1.0×10^{-9} (ζ Per) to 1.1×10^{-7} (20 Tau) with an average of about 10^{-8}. The CO, H_2, and $N(\text{H I} + H_2)$ comparisons discussed by Jenkins (1976) exhibit an even larger range of variation. A detailed interpretation of these intercomparisons is well beyond the scope of this paper.

Finally, more complete H_2 data for a number of stars which have $N(H_2)$ upper limits near 10^{19} cm^{-2} would establish whether or not a void region exists in the log $N(H_2)$ versus $E(B-V)$ plot. The most straightforward way of obtaining reliable measures of $N(0)$ and $N(1)$ for these stars would be to observe the H_2 (4, 0) $R(0)$ and $R(1)$ lines near 1050 Å. Since these lines have f-values ~ 4 times larger than the corresponding lines in the (1, 0) band, the saturation correction could probably be estimated by combining the (4, 0) and (1, 0) data.

Beyond the *Copernicus* satellite, with the possible exception of the Space Telescope, no astronomical spacecraft is currently planned that can measure interstellar H_2 at wavelengths below 1120 Å. Therefore the ultraviolet H_2 measurements of Table 1 are not likely to be extended to stars behind denser clouds or to more distant stars for some time. The recent detection of H_2 quadrupole vibrational-rotational infrared emission lines from the Orion Nebula and NGC 7027 (Gautier *et al.* 1976; Treffers *et al.* 1976) provides a new and important method for studying H_2 in dense clouds.

The completion of this extensive observing program was greatly aided by the assistance provided by the Princeton *Copernicus* staff and especially by Drs. T. Snow and D. York. Discussions with Drs. E. Jenkins, J. Mathis, and L. Spitzer helped clarify a number of troublesome points. We thank Dr. J. Black for providing the equilibrium calculations used in § III*e* in advance of publication and for several very helpful discussions. Mr. K. Feggans provided able and enthusiastic support in processing and organizing the considerable volume of spectra. B. D. S. acknowledges partial support for this study through NASA grant NSG 5100 and J. F. D. acknowledges support through the Lockheed Independent Research Program.

REFERENCES

Adams, W. S. 1949, *Ap. J.*, **109**, 354.
Allison, A. C., and Dalgarno, A. 1970, *Atomic Data*, **1**, 289.
Black, J. H. 1975, Ph.D. thesis, Harvard University.
Blanco, V. M., Demers, S., Douglass, G. G., and FitzGerald, M. P. 1970, *Pub. US Naval Obs.*, **13** (Washington: Government Printing Office).
Bless, R. C., and Savage, B. D. 1972, *Ap. J.*, **171**, 293.
Bohlin, R. C. 1975, *Ap. J.*, **200**, 402.
Bohlin, R. C., Savage, B. D., and Drake, J. F. 1977, in preparation (Paper II).
Budich, W., Bohlin, R. C., and Drake, J. F. 1976, *Corrections to the U2 Wavelength Scale between 1026 and 1110 Å* (*Copernicus* Memo.).
Carruthers, G. R. 1970, *Ap. J.* (*Letters*), **161**, L81.
Code, A. D., Holm, A. V., and Bottemiller, R. L. 1976, *Wisconsin Ap.*, No. 31.
Code, A. D., and Meade, M. R. 1976, *Wisconsin Ap., No. 30.*
Cohen, J. G. 1974, *Ap. J.*, **194**, 37.
Dalgarno, A., Black, J. H., and Weisheit, J. C. 1973, *Ap. Letters*, **14**, 77.

Dalgarno, A., and McCray, R. 1972, *Ann. Rev. Astr. Ap.*, **10**, 375.
Drake, J. F., Jenkins, E. B., Bertaux, J. L., Festou, M., and Keller, H. U. 1976, *Ap. J.*, **209**, 302.
FitzGerald, M. P. 1968, *A.J.*, **73**, 983.
Gautier, T. N., Fink, U., Treffers, R. R., and Larson, H. P. 1976, *Ap. J. (Letters)*, **207**, L129.
Glassgold, A. E., and Langer, W. D. 1974, *Ap. J.*, **193**, 73.
Habing, H. J. 1969*a*, *Bull. Astr. Inst. Netherlands*, **20**, 128.
———. 1969*b*, *Bull. Astr. Inst. Netherlands*, **20**, 177.
Hobbs, L. 1972, *Ap. J. (Letters)*, **175**, L145.
———. 1973, *Ap. J.*, **181**, 79.
Hollenbach, D. J., Chu, S-I., and McCray, R. 1976, *Ap. J.*, **208**, 458.
Hollenbach, D. J., Werner, M. W., and Salpeter, E. E. 1971, *Ap. J.*, **163**, 165.
Hughes, M. P., Thompson, A. R., and Colvin, R. S. 1971, *Ap. J. Suppl.*, **23**, 323.
Jenkins, E. B. 1971, *Ap. J.*, **169**, 25.
———. 1976, in *The Structure and Content of the Galaxy and Galactic Gamma Rays* (NASA GSFC X-662-76-154), p. 239.
Jenkins, E. B., and Savage, B. D. 1974, *Ap. J.*, **187**, 243.
Jenkins, E. B., and Shaya, E. 1977, in preparation.
Johnson, H. L. 1966, in *Ann. Rev. Astr. Ap.*, **4**, 193.
———. 1968, *Ap. J.*, **147**, 912.
Jura, M. 1975*a*, *Ap. J.*, **197**, 575.
———. 1975*b*, *Ap. J.*, **197**, 581.
Lesh, J. R. 1968, *Ap. J. Suppl.*, **16**, 371.
———. 1972, *Astr. Ap. Suppl.*, **5**, 129.
Morton, D. C., and Dinerstein, H. L. 1976, *Ap. J.*, **204**, 1.
Münch, G., and Zirin, H. 1961, *Ap. J.*, **133**, 11.
Radhakrishnan, V., Murray, J. D., Lockhart, P., and Whittle, R. P. J. 1972, *Ap. J. Suppl.*, **24**, 15.
Rickard, J. J. 1972, *Astr. Ap.*, **17**, 425.
Rogerson, J. B., Spitzer, L., Drake, J. F., Dressler, K., Jenkins, E. B., Morton, D. C., and York, D. G. 1973, *Ap. J. (Letters)*, **181**, L97.
Savage, B. D., and Bohlin, R. C. 1977, in preparation.
Savage, B. D., and Jenkins, E. B. 1972, *Ap. J.*, **172**, 491.
Smith, A. M. 1973*a*, *Ap. J. (Letters)*, **179**, L11.
Smith, L. F. 1973*b*, in *IAU Symposium No. 49, Wolf-Rayet and High-Temperature Stars*, ed. M. K. V. Bappu and J. Sahade (Dordrecht: Reidel), p. 15.
Spitzer, L. 1968, *Diffuse Matter in Space* (New York: Interscience), p. 67.
Spitzer, L., and Cochran, W. D. 1973, *Ap. J. (Letters)*, **186**, L23.
Spitzer, L., Cochran, W. D., and Hirschfeld, A. 1974, *Ap. J. Suppl.*, **28**, 373.
Spitzer, L., Drake, J. F., Jenkins, E. B., Morton, D. C., Rogerson, J. B., and York, D. G. 1973, *Ap. J. (Letters)*, **181**, L116.
Spitzer, L., and Jenkins, E. B. 1975, *Ann. Rev. Astr. Ap.*, **13**, 133.
Spitzer, L., and Morton, W. A. 1976, *Ap. J.*, **204**, 731.
Stebbins, J., Huffer, C. M., and Whitford, A. E. 1940, *Ap. J.*, **91**, 61.
Stecher, T. P., and Williams, D. A. 1967, *Ap. J. (Letters)*, **149**, L29.
Stokes, G. M., and Hobbs, L. M. 1976, *Ap. J. (Letters)*, **208**, L95.
Treffers, R. R., Fink, U., Larson, H. P., and Gautier, T. N. 1976, *Ap. J.*, **209**, 793.
van de Hulst, H. C. 1948, *Harvard Obs. Monog.*, **7**, 73.
Walborn, N. R. 1971, *Ap. J. Suppl.*, **23**, 257.
———. 1972, *Ap. J.*, **77**, 312.
———. 1973, *A.J.*, **78**, 1067.
York, D. G. 1976, *Ap. J.*, **204**, 750.
York, D. G., Drake, J. F., Jenkins, E. B., Morton, D. C., Rogerson, J. B., and Spitzer, L. 1973, *Ap. J. (Letters)*, **182**, L1.

R. C. Bohlin: NASA/Goddard Space Flight Center, Code 672, Greenbelt, MD 20771

W. Budich: Computer Sciences Corporation, 8728 Colesville Road, Silver Spring, MD 20910

J. F. Drake: Department 52-10/B202, Lockheed Palo Alto Research Laboratory, 3251 Hanover Street, Palo Alto, CA 94304

B. D. Savage: Department of Astronomy, Sterling Hall, University of Wisconsin, Madison, WI 53706